PISCES biogeochemical model

Olivier AUMONT

10/18/2005

1 Introduction

PISCES is a biogeochemical model which simulates the marine biological productivity and that describes the biogeochemical cycles of carbon and of the main nutrients (P, N, Si, Fe). Historically, this model can be seen as one of the many Monod models (*Monod*, 1942) by opposition to the quota models (*McCarthy*, 1980; *Droop*, 1983), the other big family of ocean biogeochemical model. Thus, it assumes a constant Redfield ratio and phytoplankton growth depends on the external concentration in nutrients. This choice was dictated by the computing cost as describing the internal pools of the different elements requires many more prognostic variables. And PISCES was supposed to be suited for a wide range of spatial and temporal scales, including quasi-steady state simulations on the global scale.

However, when modeling silicate, iron and/or chlorophyll, assuming constant ratios is not justified anymore as these ratios can vary a lot. For instance, the Fe/C ratio can vary by at least an order of magnitude to be compared to the N/C ratio which varies by "only" two times. Thus, in PISCES, a compromise between the two classical families of ocean model was chosen. The elemental ratios of Fe, Si and Chl are prognostically predicted based on the external concentrations of the limiting nutrients like in the quota approach. On the other hand, the phytoplankton growth rates also depends on these external concentrations as in the Monod approach.

Historically, the development of this model started in 1997 with the release of the P3ZD model which was a simple NPZD model with semi-labile DOM (*Aumont*, 1998; *Aumont et al.*, 2002). Phytoplankton growth rate was only limited by one nutrient, basically phosphate. However, many deficiencies in this model, especially in the HNLC regions, justified the development, in 1999, of a more complex model including three limiting nutrients (Fe, Si, P), two phytoplankton and two zooplankton size-classes. This model was called HAMOCC5 (*Aumont et al.*, 2003) as it was based on HAMOCC3.1 (*Six and Maier-Reimer*, 1996) and used in the LSG model (*Maier-Reimer et al.*, 1993). The embedding of this code in the ocean model OPA (*Madec et al.*, 1998) required some major changes and improvements, partly because of the much finer vertical resolution. Beside the numerical schemes, these changes were mostly an improved treatment of the optics and the splitting of the particulate organic matter into two different size-classes. All these changes and the major recodings it required lead us to adopt a new name for the model: PISCES. This name can be translated as fishes from Latin. It can also be considered as an acronym, but its meaning is much less poetic and will not be explained here as it is not really essential.

Since 2001, this model has undergone active developments. In 2004, a stable release of the model is made available to the community on the OPA website (www.lodyc.jussieu.fr/opa). It can be freely used and changed by anybody after subscription to the OPA system. Currently, this model is being coupled to OPA only. However, a beta version of the model coupled to ROMS can be obtained by sending an email to this address (olivier.aumont@ird.fr). The rest of this document describes the main aspects of the model. If you have any comments or suggestions, send me an email (olivier.aumont@ird.fr). I do not promise to take them into account (or even to read the mail) but I'll do my best.

2 Model description

PISCES has currently twenty-four compartments (see figure 1). There are five modeled limiting nutrients for phytoplankton growth: Nitrate and Ammonium, Phosphate, Silicate and Iron. It should be mentioned that phosphate and nitrate+ammonium are not really independent nutrients in PISCES. They are linked by constant Redfield ratios but the nitrogen pool undergoes nitrogen fixation and denitrification. This means that if the latter two processes are set to zero and if the sizes of the nitrogen and phosphorus pools are identical, the distributions of both nutrients should be exactly the same.

Four living compartments are represented: two phytoplankton size-classes/groups corresponding to nanophytoplankton and diatoms, and two zooplankton size classes which are microzooplankton and mesozooplankton. For phytoplankton, prognostic variables are total biomass, the iron, chlorophyll and silicon contents. This means that the Fe/C, Chl/C and Si/C ratios of both phytoplankton groups are fully predicted by the model. For zooplankton, only the total biomass is modeled. For all species, the C/N/P/O2 ratios are supposed constant and are not allowed to vary. In PISCES, the Redfield ratio -O/C/N/P is set to 172/122/16/1 (*Takahashi et al.*, 1985). In addition, the Fe/C ratio of both zooplankton groups is kept constant. No silicified zooplankton is assumed. The bacterial pool is not yet explicitly modeled.

There are three non-living compartments: semi-labile dissolved organic matter, small and big sinking particles. As for the living compartments, the C, N and P pools are not distinctly modeled. Thus, constant Redfield ratios are imposed for C/N/P. However, the iron, silicon and calcite pools of the particles are explicitly modeled. As a consequence, their ratios are allowed to vary. The sinking speed of the particles is not altered by their content in calcite and biogenic silicate ("The ballast effect", (*Honjo*, 1996; *Armstrong et al.*, 2002)). The latter particles are assumed to sink at the same speed than big organic matter particles. All the non-living compartments experience aggregation due to turbulence and differential settling.

In addition to the ecosystem model, PISCES also simulates dissolved inorganic carbon, total alkalinity and dissolved oxygen. The latter tracer is also used to define the regions where oxic or anoxic remineralization takes place.

3 Model equations

The reader should be aware that in the following equations, the conversion ratios between the different elements (Refield ratios) have been often omitted except when particular parameterizations are defined. All phytoplankton and zooplankton biomasses are in carbon units except for the silicon, chlorophyll and iron content of phytoplankton. Finally, all parameters and their standard values in PISCES are listed in Table 1 at the end of this section.
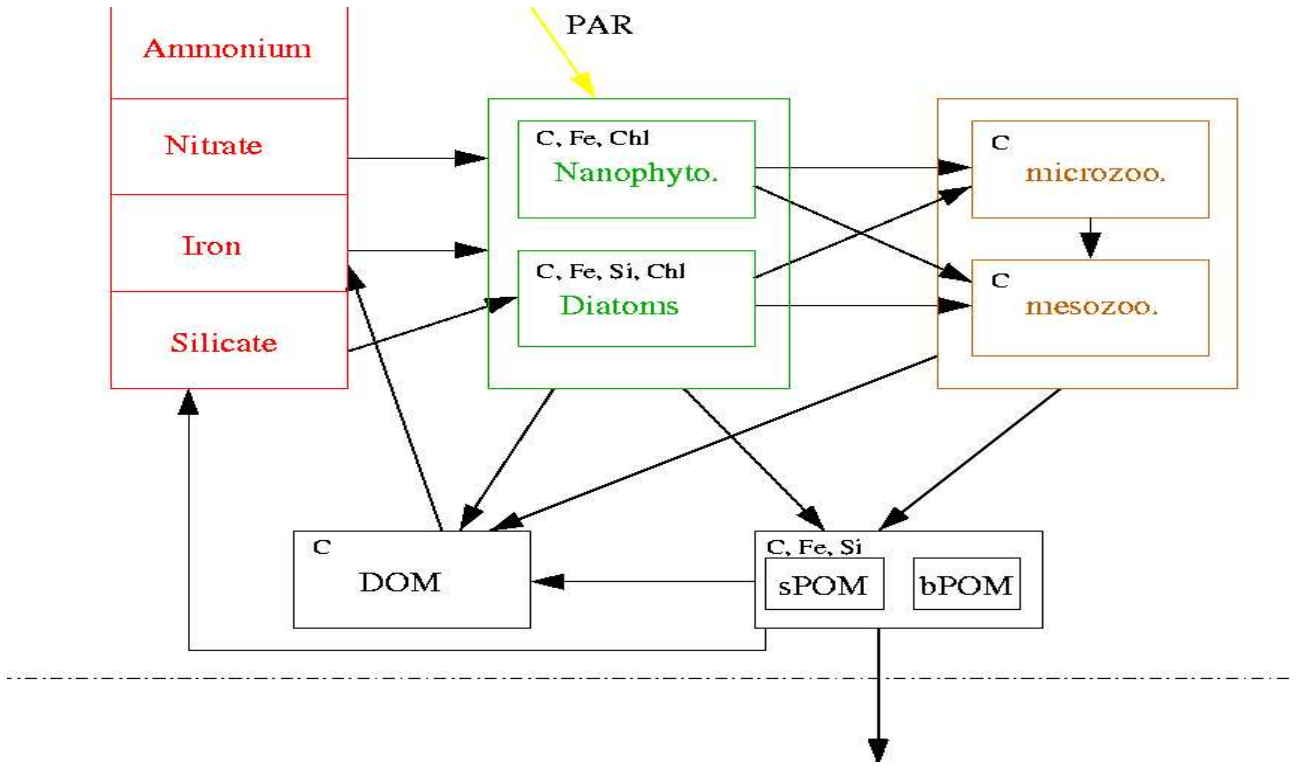
Figure 1: Architecture of PISCES. This figure only shows the ecosystem model omitting thus oxygen and the carbonate system. The element which are explicitly modeled are indicated in the left corner of each box.

3.1 Equation for nanophytoplankton

$$\frac{\partial P}{\partial t} = (1 - \delta^P)\mu^P P - m^P \frac{P}{K_P + P} P - w_p^P P^2 - g^Z(P)Z - g^Z(P)M \tag{1}$$

The production terms for nano/picophytoplankton is defined by :

$$\mu^P = \mu_P \left(1 - e^{\frac{\alpha^P (\frac{Chl}{C})^P PAR}{\mu_P L_{lim}^P}} \right) L_{lim}^P \tag{2}$$

where $\mu_P = ab^{cT}$ and where the limitations terms are defined as follows:

$$
\begin{aligned}
L_{po4}^P &= \frac{PO_4}{K_{po4}^P + PO_4} \\
L_{fe}^P &= \frac{Fe}{K_{Fe}^P + Fe} \\
L_{no3}^P &= \frac{K_{nh4}^P NO_3}{K_{no3}^P K_{nh4}^P + K_{nh4}^P NO_3 + K_{no3}^P NH_4} \\
L_{nh4}^P &= \frac{K_{no3}^P NH_4}{K_{no3}^P K_{nh4}^P + K_{nh4}^P NO_3 + K_{no3}^P NH_4} \\
L_{lim}^P &= \min(L_{po4}^P, L_{Fe}^P, L_{no3}^P + L_{nh4}^P)
\end{aligned}
\tag{3}
$$

The choice of the half-saturation constants is rather difficult as observations show that they can very by several orders of magnitude (e. g., *Perry*, 1976; *Sommer*, 1986; *Donald et al.*,

3

1997). However, in general, these constants increase with the size of the phytoplankton cell as a consequence of a smaller surface-to-volume ratio (diffusive hypothesis) (*Eppley et al.*, 1969). Thus, diatoms will tend to have larger half-saturation constants than nanophytoplankton. But, in PISCES, phytoplankton is modeled by only two compartments, each of them encompassing thus a large size spectrum. Experiments performed with model have shown that results are especially sensitive to the choice of the iron half-saturation constants, and less to the other constants (with the exception perhaps of silicate). This is not surprising as over most of the ocean, the seawater iron concentrations are close to these constants.

Following these remarks, it appeared not appropriate to keep the iron half-saturations constant. It was then decided to make them vary with the phytoplankton biomass of each compartment. It is assumed that they increase with biomass based on the observations showing that the increase in biomass is generally due to the addition of larger size classes of phytoplankton (e.g., *Raimbault et al.*, 1988; *Armstrong*, 1994; *Hurtt and Armstrong*, 1996):

$$
\begin{aligned}
P_1 &= \min(P, P_{max}) \\
P_2 &= \max(0, P - P_{max}) \\
K_{Fe} &= \frac{K_{Fe}^{min} P_1 + K_{Fe}^{max} P_2}{P_1 + P_2}
\end{aligned}
\tag{4}
$$

The three parameters in this equation (P_{max}, K_{Fe}^{min}, and K_{Fe}^{max}) can be independently specified for each phytoplankton group.

The distinction between new production based on nitrate and regenerated production based on ammonium is computed as follows (*O'Neill et al.*, 1989):

$$
\begin{aligned}
\mu_{no3}^P &= \mu^P \frac{L_{no3}^P}{L_{no3}^P + L_{nh4}^P} \\
\mu_{nh4}^P &= \mu^P \frac{L_{nh4}^P}{L_{no3}^P + L_{nh4}^P}
\end{aligned}
\tag{5}
$$

The vertical attenuation of PAR is computed using a simplified version of the full spectral model of *Morel and Berthon* (1989). Only three wavelengths are considered with equal contribution to the total visible light at the surface (Red, Green, Blue). The PAR is supposed to be a constant fraction of the total shortwave radiative flux (0.43) at the sea surface.

The nanophytoplankton aggregation term w_P^P depends on the shear rate as the main driving force for aggregation is the local turbulence. Rather arbitrarily, this shear rate is set to 1 s^{-1} in the mixed layer and to 0.01 s^{-1} below. This means that the aggregation is reduced by a factor of 100 below the mixed layer.

3.2 Equation for diatoms

$$
\frac{\partial D}{\partial t} = (1 - \delta^D)\mu^D D - m^D \frac{D}{K_D + D} D - w_p^D D^2 - g^Z(D)Z - g^M(D)M
\tag{6}
$$

The production terms for diatoms are defined as for nanophytoplankton except that the limitations terms also include Si:

$$
\begin{aligned}
L_{Si}^D &= \frac{Si}{K_{Si}^D + Si} \\
L_{lim}^D &= \min(L_{po4}^D, L_{Fe}^D, L_{no3}^D + L_{nh4}^D, L_{Si}^D)
\end{aligned}
\tag{7}
$$

4

As for iron, the half-saturation factor can vary significantly over the ocean. In the tropical and temperate regions, this factor is around 1 μM whereas values as high as 88.7 μM have been measured for Antarctic species (*Sommer*, 1986; *Martin-Jézéquel et al.*, 2000). When plotted against maximum local yearly concentration of silicate, a crude relationship can be inferred (*Pondaven et al.*, 1998):

$$K_{Si}^D = K_{Si}^{min} + K_{Si}^{max} \frac{Si_{max}^2}{K_{Si}^2 + Si_{max}^2} \tag{8}$$

In this equation, Si_{max} represents the maximum yearly silicate concentration.

The diatoms aggregation term w_p^D is increased in case of nutrient limitation because it has been shown that diatoms cells sink out more rapidly in case of nutrient stress (e.g., *Brzezinski and Nelson*, 1988; *Muggli et al.*, 1996). Even, if this increased sinking rate is not strictly speaking aggregation, the resulting higher loss rate is mimicked in the model by enhanced aggregation loss:

$$w_p^D = w_p^{min} + w_p^{max} \times (1 - L_{lim}^D) \tag{9}$$

Furthermore as for nanophytoplankton, the aggregation is multiplied by the shear rate.

3.3 Equation for chlorophyll and iron in phytoplankton

Chlorophyll for both phytoplankton groups is parametrized using the photoadaptative model f *Geider et al.* (1998):

$$\begin{aligned}
\frac{\partial I^{Chl}}{\partial t} &= \rho_{Chl}^I (1 - \delta^I)\mu^I I - m^I \frac{I}{K_I + I} I^{Chl} \\
&\quad - w_p^I I I^{Chl} - g^Z(I)\theta_{Chl}^I Z - g^M(I)\theta_{Chl}^I M
\end{aligned} \tag{10}$$

where I is the phytoplankton class and θ_{Chl}^I is the chlorophyll-to-carbon ratio of the considered phytoplankton class. ρ_{Chl}^I represents the ratio of energy assimilated to energy absorbed as defined by *Geider et al.* (1996):

$$\rho_{Chl}^I = \theta_{Chl,max}^I \frac{144\mu^I I}{\alpha^I \times PAR \times I^{Chl}} \tag{11}$$

In this equation, 144 is the square of the molar mass of C and is used to convert from mol to mg as the standard unit for Chl is generally in mg Chlm^{-3}.

For the iron content of phytoplankton, a similar approach has been adopted as iron is mostly related to the photosynthetic apparatus. Thus, the equations predicting the iron content of both phytoplankton groups are exactly equivalent to equation 10. This parameterization produces variations of the Fe/C ratios which are consistent with the observations: these ratios decrease with light and with the nutrient stress including iron (*Sunda and Huntsman*, 1997).

3.4 Equation for the silicon content of diatoms

$$\begin{aligned}
\frac{\partial D^{Si}}{\partial t} &= (1 - \delta_2)\mu^D \left(\frac{Si}{C}\right)^{opt} D - m^D \frac{D}{K_D + D} D^{Si} \\
&\quad - w_P^D D D^{Si} - (g^Z(D)Z + g^M(D)M)\left(\frac{D^{Si}}{D}\right)
\end{aligned} \tag{12}$$

5

Where the $(\frac{Si}{C})^{opt}$ ratio is diagnostically computed.

The elemental ratio Si/C (or Si/N) have been observed to vary by a factor of about 4 over the global ocean with a mean value around 0.14±0.13 mol/mol (*Sarthou et al.*, 2005). Light, N, P, or Fe stress has been demonstrated to lead to heavier silicification (e.g., *Takeda*, 1998; *Franck et al.*, 2000; *Martin-Jézéquel et al.*, 2000). It has been suggested that these elevated elemental ratios result from the physiological adaptation of the silicon uptake by the cell depending on the growth rate and on the G2 cycle phase during which Si is incorporated (*Martin-Jézéquel et al.*, 2000; *Claquin et al.*, 2002). Lighter silicification can only result from silicate limitation.

We model the variations of the Si/C ratio following the parameterization proposed by *bucciarelli et al., 2002, unpublished manuscript*:

$$
\begin{aligned}
F_{Lim}^{Si} &= \min((1 - e^{\frac{\alpha^D (\frac{Chl}{C})^D PAR}{\mu_D L_{lim}^D}}), L_{po4}^D, L_{Fe}^D, L_{no3}^P + L_{nh4}^P) \\
\left(\frac{Si}{C}\right)^{opt} &= 0.14 L_{Si}^D (5.4 e^{F_{Lim}^{Si}} + 1.13)
\end{aligned}
\tag{13}
$$

Relative to the original parameterization, a additional limitation term by Si has been added to produce a lighter silicification in case of Si exhaustion.

3.5 Equation for microzooplankton

$$
\frac{\partial Z}{\partial t} = e^Z (g^Z(P) + g^Z(D) + g^Z(POC_s))Z_1 - r^Z \frac{Z}{K_Z + Z} Z
\tag{14}
$$

The grazing on each species N is defined following *Fasham et al.* (1993):

$$
g^Z(N) = g^Z \frac{p_N^Z N}{K_G^Z + \sum_I (p_I^Z I)}
\tag{15}
$$

where I denotes all the resources microzooplankton can graze on and p_N^Z is the preference microzooplankton has for N:

$$
p_N^Z = \frac{\rho_N}{\sum_I (\rho_I)}
\tag{16}
$$

The grazing rate g^Z depends on temperature following exactly the same relationship than phytoplankton. It means that we assume a Q_{10} for microzooplankton of about 1.9. We have also adopted this temperature dependency for respiration/mortality.

A special treatment is applied on both types of phytoplankton:

- For nanophytoplankton, a minimum threshold is assumed based on observations showing that below a certain small chlorophyll concentration, grazing ceases. This threshold is generally of the order of 0.03 mg Chl l^{-1} (e.g, *Strom et al.*, 2000). Thus, for nanophytoplankton, the concentration in the grazing equation (see Eq. 15) is max(P-P_{min},0) instead of P.

- For diatoms, observations show that the biomass increases by the addition of larger cells which escape grazing by microzooplankton. Thus, we assume in PISCES that above a certain concentration, the diatoms excess is unavailable to microzooplanton. The diatoms concentration in Eq. 15 is then min(D_{max},D).

6

3.6   Equation for mesozooplankton

$$\frac{\partial M}{\partial t} = e^M(g^M(P) + g^M(D) + g^M(Z) + g^M(POC_s) + g^M(POC_b))M$$
$$-r^M\frac{M}{K_M + M}M - m^M M^2 \tag{17}$$

The parametrization for the grazing on multiple resources differs from the one adopted for microzooplankton (compare with equation 15) (e.g., *Frost*, 1987; *Moloney and Field*, 1991):

$$g^M(N) = g^M\frac{p_N^M N}{K_G^M + \sum_I(p_I^M I)} \tag{18}$$

This parameterization implies that mesozooplankton always predominantly grazes on the most preferred prey (no-switching parameterization). It avoids the maintenance of high-standing stocks of mesozooplankton in the case of small-cells dominated ecosystem (for instance, in oligotrophic regimes) which would happen with the parameterization adopted for microzooplankton.

In addition to the "conventional" concentration-dependent grazing described by equation 15, flux-feeding is also accounted for in PISCES. This type of grazing has been shown to be potentially very important for the fate of particles in the water column below the euphotic zone (*Dilling and Alldredge*, 2000; *Stemmann et al.*, 2004). Flux feeding depends on the flux and thus, on the product of the concentration and of the sinking speed. In PISCES, only the largest particles experience this type of grazing as they are the fastest sinking material:

$$g^M(POC_b) = g_{FF}^M w^{POC_b}POC_b \tag{19}$$

In the equation for mesozooplankton, the term with a square dependency to mesozooplankton does not depict aggregation but grazing by the higher, non-resolved trophic levels. All terms in the equation driving the temporal evolution of mesozooplankton depend on temperature using a Q_{10} of 2.14 (*Buitenhuis et al.*, 2005).

3.7   Equation for DOC

$$\frac{\partial DOC}{\partial t} = \delta^P\mu^P P + \delta^D\mu^D D + (1 - \epsilon^Z)r^Z\frac{Z}{K_Z + Z}Z$$
$$+(1 - \epsilon^M)r^M\frac{M}{K_M + M}M + (1 - \sigma^Z - e^Z)$$
$$(1 - \gamma^Z)(g^Z(P) + g^Z(D) + g^Z(POC_s))Z$$
$$+(1 - \sigma^M - e^M)(1 - \gamma^M)(g^M(P) + g^M(D)$$
$$+g^M(Z) + g^M(POC_s) + g^M(POC_b))M + \lambda_{POC}^\star POC_s$$
$$-\lambda_{DOC}^\star DOC - \Phi_{agg}^{DOC \to POC_s} - \Phi_{agg}^{DOC \to POC_b} \tag{20}$$

where the remineralization rate of DOC is parameterized as follows:

$$\lambda_{DOC}^\star = \lambda_{DOC}L_{lim}^{bac}0.7(Z + 2M)\min(1, \frac{120m}{z})$$
$$L_{Lim}^{bac} = L_{lim}^P\frac{DOC}{K_{DOC}^{bac} + DOC} \tag{21}$$

Remineralization of DOC can be either oxic or anoxic depending on the local oxygen concentration. The splitting between the two types of organic matter degradation is performed using a factor $\Delta(O_2)$ comprised between 0 and 1 (see section 3.12 for the formulation of this factor). Implicitly, this assumes that the degradation rates for respiration and denitrification are identical.

In the previous equation, 0.7(Z+2M) is a proxy for the bacterial concentration. This relationship has been constructed from a version of PISCES that includes an explicit description of the bacterial biomass. Below 120m, this proxy is kept constant and is set to its value at 120m. The terms Φ denote aggregation processes and are described hereafter (see Equation 23).

3.8 Equation for the two size classes of POC

$$
\begin{aligned}
\frac{\partial POC_s}{\partial t} &= \sigma^Z (\sum_N g^Z(N))Z - g^Z(POC_s)Z \\
&+ (1 - 0.5 R_{CaCO3}) \left(m^P \frac{P}{K_P + P} P + w_P^P P^2 \right) \\
&+ 0.5 m^D \frac{D}{K_D + D} D + \epsilon^Z r^Z \frac{Z}{Z_Z + Z} Z - \lambda^\star_{POC} POC_s \\
&- w^{POC_s} \frac{\partial POC_s}{\partial z} + \Phi^{DOC \to POC_s}_{agg} - \Phi^{POC_s \to POC_b}_{agg} \\
\frac{\partial POC_b}{\partial t} &= \sigma^M (\sum_N g^M(N))M + \epsilon^M r^M \frac{M}{K_M + M} M + m^M M^2 \\
&+ 0.5 R_{CaCO3} \left(m^P \frac{P}{K_P + P} P + w_P^P P^2 \right) + 0.5 m^D \frac{D}{K_D + D} D \\
&+ w_P^D D^2 - \lambda^\star_{POC} POC_b - w^{POC_b} \frac{\partial POC_b}{\partial z} + \Phi^{DOC \to POC_b}_{agg} \\
&+ \Phi^{POC_s \to POC_b}_{agg}
\end{aligned}
\tag{22}
$$

The fate of mortality and aggregation of nanophytoplankton depends on the proportion of the calcifying organisms (R_{CaCO3}). We assume that 50% of the organic matter of the calcifiers is associated with the shell. Since calcite is significantly denser than organic matter, 50% of the dying calcifiers biomass is routed to the fast sinking particles. The same is assumed for the mortality of diatoms as a consequence of the denser density of biogenic silica.

Like for DOC, the Φ terms represent aggregation processes. In PISCES, differential sedimentation and turbulence coagulation mechanisms are considered. Differential sedimentation is omitted for DOC as this term is almost negligible compared to turbulence.

$$
\begin{aligned}
\Phi^{DOC \to POC_s}_{agg} &= \phi_1^{DOC} \operatorname{sh} DOC^2 + \phi_2^{DOC} \operatorname{sh} DOC \, POC_s \\
\Phi^{DOC \to POC_b}_{agg} &= \phi_3^{DOC} \operatorname{sh} DOC \, POC_b \\
\Phi^{POC_s \to POC_b}_{agg} &= \phi_1^{POC_s} \operatorname{sh} POC_s^2 + \phi_2^{POC_s} \operatorname{sh} POC_b \, POC_s \\
&+ \phi_3^{POC_s} POC_s^2 + \phi_4^{POC_s} POC_b \, POC_s
\end{aligned}
\tag{23}
$$

In these equations, sh is the shear rate. It is set to 1 s^{-1} in the mixed layer and to 0.01 s^{-1} elsewhere. The coefficients ϕ were obtained by integrating the standard curvilinear kernels for collisions over the size range of each organic matter pool assuming a power size spectra

(see *Kriest* (2002)) for a description of this computation). The power value of this spectra has been arbitrarily set to 3.28. This number is derived assuming a fractal dimension of 2.28 for the aggregates and a constant mass distribution over the size range of the considered particle size-class.

The degradation rate $\lambda^{\star}_{POC}$ depends on temperature with a Q_{10} of about 1.9.

Furthermore, many observations have shown that the mean sinking speed of the particulate organic matter increases with depth (e.g., *Berelson*, 2002). This increase is parameterized in PISCES as follows:

$$w^{POC} = w^{POC}_{min} + (w^{POC}_{max} - w^{POC}_{min}) \max(0, \frac{z - z_{mel}}{2000m}) \tag{24}$$

This equation is used only for big POC. The parameters in this equation have been adjusted using a model of aggregation/disaggregation with multiple size classes (*Gehlen et al.*, 2005). We have not yet included a ballasting effect due to the higher density of biogenic silica or calcite (*Armstrong et al.*, 2002).

3.9 Equation for biogenic silica

$$\begin{aligned}
\frac{\partial BSi}{\partial t} &= m^D \frac{D}{K_D + D} D^{Si} + w^D_P DD^{Si} + \left(\frac{D^{Si}}{D}\right)(g^Z(D)Z + g^M(D)M) \\
&\quad - \lambda^{\star}_{BSi} BSi - w^{POC_b} \frac{\partial BSi}{\partial z}
\end{aligned} \tag{25}$$

The dissolution rate of BSi depends on in situ temperature and on saturation following the parameterization proposed by *Ridgwell et al.* (2002):

$$\begin{aligned}
Si_{eq} &= 10^{6.44 - \frac{968}{T + 273.15}} \\
Si_{sat} &= \frac{Si_{eq} - Si}{Si_{eq}} \\
\lambda^{\star}_{BSi} &= \lambda_{BSi}\left[0.225\left(1 + \frac{T}{15}\right)Si_{sat} + 0.775\left(\left(1 + \frac{T}{400}\right)^4 Si_{sat}\right)^9\right]
\end{aligned} \tag{26}$$

3.10 Equations for particulate organic iron

To make the document clearer, the equations are not detailed here. The reader could refer to the equations for particulate organic carbon (see Equations 22) as the sources and sinks are pretty much the same as for PFe.

3.11 Equation for calcite

In PISCES, calcium carbonate is supposed to be only in the form of calcite. Thus, aragonite is not considered, for instance, for the computation of the chemical dissolution in the water column.

$$\begin{aligned}
\frac{\partial CaCO_3}{\partial t} &= R_{CaCO3}(0.5(\sigma^Z g^Z(P) + \sigma^M g^M(P)M) + w^P_P P^2 \\
&\quad + m^P \frac{P}{K_P + P} P) - \lambda^{\star}_{CaCO3} CaCO_3 - w^{POC_b} \frac{\partial CaCO_3}{\partial z}
\end{aligned} \tag{27}$$

In this equation, the rain ratio R_{CaCO3} is variable. The proportion of calcifying phytoplankton is generally very low in oligotrophic regions. When the nanophytoplankton blooms, the dominant species are often calcifiers. To mimic these very general considerations, we propose the following parameterizations which is similar to that of *Moore et al.* (2002):

$$R_{CaCO3} = R^\star_{CaCO3} L^P_{lim} \max\left(0.0001, \frac{T}{2+T}\right) \max\left(1, \frac{P}{2}\right) \tag{28}$$

The rain ratio is not allowed to fall below 0.01 and to exceed 0.8.

Only half of the grazed shells is routed to sinking calcite. The rest is supposed to dissolve in the acidic guts of zooplankton (*Jansen and Wolf-Gladrow*, 2001). This dissolution is still debated. However, observations tend to show that a significant proportion of the sinking shells is lost in the upper ocean, whether during grazing or by other mechanisms (*Milliman et al.*, 1999).

The dissolution rate constant is defined following *Maier-Reimer* (1993):

$$\begin{aligned}
\Delta CO3 &= \max(0, CO3^{2-}_{sat} - CO3^{2-}) \\
\lambda^\star_{CaCO3} &= \lambda_{CaCO3}\frac{\Delta CO3}{K_{CaCO3} + \Delta CO3}
\end{aligned} \tag{29}$$

This means that no dissolution is allowed in case of over-saturation. On the other hand, dissolution increases with the undersaturation level.

3.12 Equations for the different modeled nutrients

$$\begin{aligned}
\frac{\partial PO_4}{\partial t} =\ & -\mu^P P - \mu^D D + \lambda^\star_{DOC} DOC \\
& + (1 - \sigma^Z - e^Z)\gamma^Z(g^Z(P) + g^Z(D) + g^Z(POC_s))Z \\
& + (1 - \sigma^M - e^M)\gamma^M(g^M(P) + g^M(D) + g^M(Z) \\
& + g^M(POC_s) + g^M(POC_b))M
\end{aligned} \tag{30}$$

$$\frac{\partial NO_3}{\partial t} = -\mu^P_{no3} P - \mu^D_{no3} D + Nitrif - Denit \tag{31}$$

$$\begin{aligned}
\frac{\partial NH_4}{\partial t} =\ & -\mu^P_{nh4} P - \mu^D_{nh4} D + \lambda^\star_{DOC} DOC - Nitrif + Nfix \\
& + (1 - \sigma^Z - e^Z)\gamma^Z(g^Z(P) + g^Z(D) + g^Z(POC_s))Z \\
& + (1 - \sigma^M - e^M)\gamma^M(g^M(P) + g^M(D) + g^M(Z) \\
& + g^M(POC_s) + g^M(POC_b))M
\end{aligned} \tag{32}$$

$$\frac{\partial Si}{\partial t} = -(1 - \delta^D)\mu^D\left(\frac{Si}{C}\right)D + \lambda^\star_{BSi} BSi \tag{33}$$

$$\begin{aligned}
\frac{\partial Fe}{\partial t} =\ & -(1 - \delta^P)\mu^P_{Fe} P - (1 - \delta^D)\mu^D_{Fe} D + \left(\frac{Fe}{C}\right)^{zoo} \\
& \left((1 - \epsilon^Z)r^Z\frac{Z}{K_Z + Z}Z + (1 - \epsilon^M)r^M\frac{M}{K_M + M}M\right) \\
& + (1 - e^Z - \sigma^Z)[\left(\frac{P^{Fe}}{P}\right)g^Z(P) + \left(\frac{D^{Fe}}{P}\right)g^Z(D) + \left(\frac{PFe_s}{POC_s}\right)g^Z(POC_s)]Z \\
& + (1 - e^M - \sigma^M)[\left(\frac{P^{Fe}}{P}\right)g^M(P) + \left(\frac{D^{Fe}}{P}\right)g^M(D)
\end{aligned}$$

10

$$+ \left(\frac{PFe_s}{POC_s}\right) g^M(POC_s) + \left(\frac{Fe}{C}\right)^{zoo} g^M(Z) + \left(\frac{PFe_b}{POC_b}\right) g^M(POC_b)]M$$
$$+\lambda^\star_{POC} PFe_s - \lambda_{scav} Fe' \tag{34}$$

In the latter equation, some additional terms are added in the code to ensure iron conservation during grazing. These terms are needed because of the differences in the $\frac{Fe}{C}$ ratios between the preys and the grazers. However, to keep the equations as clear as possible, they have not been displayed here.

Nitrification (Nitrif) corresponds to the conversion of ammonium to nitrate due to bacterial activity. It is assumed to be photoinhibited (e.g., *Horrigan et al.*, 1981; *Yoshioka and Saijo*, 1984) and reduced in suboxic waters:

$$Nitrif = \lambda_{NH4} \frac{1}{1+PAR}(1 - \Delta(O_2))NH_4 \tag{35}$$

where $\Delta(O_2)$ varies between 0 (oxic conditions) and 1 (anoxia) according to:

$$\Delta(O_2) = \min\left(1, 0.4\frac{\max(0, 6 - O_2)}{O_2^{min} + O_2}\right) \tag{36}$$

When the waters become suboxic, nitrate instead of oxygen is consumed for the remineralization of organic matter (denitrification):

$$Denit = R_{NO3}\lambda^\star_{DOC}\Delta(O_2)DOC \tag{37}$$

where the N/C stoichiometric ratio R_{NO3} is set to 0.8 (*Middelburg et al.*, 1996; *Soetaert et al.*, 2000). From equation 36, it comes that denitrification stops for oxygen concentration above 6 μM (*Lipschultz et al.*, 1990).

Finally, nitrogen fixation is parameterized in PISCES in a very crude way as follows:

$$\begin{aligned} Nfix_{pot} &= \mu^P \max(0, \mu_P - \mu_P(20^oC))(1 - L^P_{no3} - L^P_{nh4})L^D_{fe} \\ Nfix &= \frac{\int_{A,t} Denit}{\int_{A,t} Nfix_{pot}} Nfix_{pot} \end{aligned} \tag{38}$$

where $\int_{A,t}$ means spatial and temporal integration over a year and the ocean area.

This very crude parameterization is based on the following assumptions:

- Nitrogen fixation is restricted to warm waters above 20°C

- Nitrogen fixation is restricted to area with insufficient nitrogen

- Nitrogen fixation requires iron

- Nitrogen fixation is restricted to the sea surface

- To ensure N conservation in the ocean, annual total nitrogen fixation should balance denitrification.

Thus, from the last point of this list of hypotheses, it comes that the maximum rate of nitrogen fixation is diagnosed from denitrification.

Dissolved iron is assumed to be in the form of free inorganic iron Fe' and of "complexed" iron FeL. Both forms of iron are assumed to be equally susceptible to consumption by phytoplankton despite recent observations suggest that this may be not the case (*Nishioka and Takeda*, 2000;

Chen and Wang, 2001; *Chen et al.*, 2003). As in *Parekh et al.* (2004), we assume that the complexation reaction is rapid enough to be at equilibrium. Thus, the chemical speciation of iron is deduced from the three following equations:

$$
\begin{aligned}
L_T &= FeL + L' \\
Fe &= FeL + Fe' \\
K_{FeL} &= \frac{FeL}{L'Fe'}
\end{aligned}
\tag{39}
$$

The chemical equilibrium constant K_{FeL} is computed from the formulation proposed by *Liu and Millero* (2002). The total ligand concentration L_T is supposed constant over the global ocean and is set as a parameter of the model.

The free form of dissolved iron Fe' is the only form of iron that is supposed to be susceptible to scavenging. The scavenging rate of iron is made dependent upon the particulate load of the seawater as follows (e.g., *Honeyman et al.*, 1988; *Parekh et al.*, 2004):

$$
\lambda_{Fe}^\star = \lambda_{Fe}^{min} + \lambda_{Fe}(POC_s + POC_b + CaCO_3 + BSi)
\tag{40}
$$

Implicitly, in this equation, it is assumed that the affinity of iron for the different types of particles is the same.

3.13   Equations for the carbonate system

$$
\begin{aligned}
\frac{\partial DIC}{\partial t} &= -\mu^P P - \mu^D D + \lambda_{DOC}^\star DOC + G^Z Z + G^M M \\
&\quad + \lambda_{CaCO3}^\star CaCO3 - P_{CaCO3}
\end{aligned}
\tag{41}
$$

$$
\begin{aligned}
\frac{\partial TALK}{\partial t} &= R_{N/C}(\mu^P P + \mu^D D - \lambda_{DOC}^\star DOC - G^Z Z - G^M M) \\
&\quad + 2\lambda_{CaCO3}^\star CaCO3 - 2P_{CaCO3}
\end{aligned}
\tag{42}
$$

$$
G^M = (1 - \sigma^M - e^M)\gamma^M \sum_I g^M(I)
\tag{43}
$$

$$
G^Z = (1 - \sigma^Z - e^Z)\gamma^Z \sum_I g^Z(I)
\tag{44}
$$

$$
\begin{aligned}
P_{CaCO3} &= R_{CaCO3}[0.5(\sigma^Z g^Z(P) + \sigma^M g^M(P)M) + w_P^P P^2 \\
&\quad + m^P \frac{P}{K_P + P}P]
\end{aligned}
\tag{45}
$$

All terms in the above equations have been described previously in this document. In addition to these biogeochemical fluxes, the ocean exchanges CO_2 with the atmosphere at the sea-surface. The gas exchange coefficient is computed from the relationship proposed by *Wanninkhof* (1992). The carbonate chemistry follows the OCMIP protocols (see the OCMIP website for more information at www.ipsl.jussieu.fr/OCMIP) except that it has been simplified to reduce the computing cost: alkalinity only includes carbonate, borate and water (H^+, OH^-).

Atmospheric pCO_2 is set as an external tunable parameter via a namelist (see Table 2). Its value is uniform over the global ocean (no spatial gradient) and is not allowed to vary with time during a simulation. This means that PISCES does not include an interactive atmospheric box or model. However, by performing successive simulations of one year, it is possible to alter the atmospheric pCO_2 at the beginning of each new simulated year, for instance, to track the increase due to the anthropogenic activities.

3.14 Equation for oxygen

The temporal evolution of oxygen is computed as follows:

$$
\begin{aligned}
\frac{\partial O2}{\partial t} = {} & R^1_{O/C}(\mu^P_{nh4}P + \mu^D_{nh4}D - \lambda^\star_{DOC}(1 - \Delta(O2))DOC - G^Z Z - G^M M) \\
& - R^2_{O/C} Nitrif + (R^1_{O/C} + R^2_{O/C})(\mu^P_{no3}P + \mu^D_{no3}D)
\end{aligned}
\tag{46}
$$

In this equation, the stoichiometric ration $R^1_{O/C}$ represents the change in oxygen relative to carbon when ammonium is convert to organic matter whereas $R^2_{O/C}$ denotes the consumption in oxygen during nitrification. Their values have been set respectively to 140/122 and 32/122 so that the sum equals the ratio proposed by *Takahashi et al.* (1985).

3.15 External supply of nutrients

Nutrients are supplied to the ocean from three different sources: atmospheric dust deposition, rivers and sediment mobilization. Iron deposition from the atmosphere has been estimated from the climatological monthly maps of dust deposition simulated by the model of *Tegen and Fung* (1995). Iron content and surface solubility are set at constant values of 3.5% and 2% respectively (e.g., *Fung et al.*, 2000; *Jickells and Spokes*, 2001; *Moore et al.*, 2004). One it has left the surface layer, particulate inorganic iron from dust is still experiencing dissolution. The dissolution rate is computed assuming that mineral particles sink at 5 m/day and that about 0.0002% of the particulate iron dissolves in a day (*Bonnet and Guieu*, 2004). This is equivalent to a remineralization length scale of 25000m, of the same order than the length scale prescribed for the same process by *Moore et al.* (2004).

Atmospheric deposition of Si is also considered following (*Moore et al.*, 2002). River discharge of carbon is taken from the Global Erosion Model (GEM) of *Ludwig et al.* (1996), neglecting the POC delivery as most of it is lost in the estuaries and in the coastal zone (*Smith and Hollibaugh*, 1993). GEM provides annual mean river discharge of DOC and DIC. Fe, N, P and Si supplies are derived from this model output by considering constant Fe/P/N/Si/C ratios in the rivers. These ratios have been computed from the global estimates by *Meybeck* (1993) for N and P, by *Tréguer et al.* (1995) for Si and by *de Baar and de Jong* (2001) for Fe.

Reductive mobilization of iron from marine sediments have been recognized as a significant source to the ocean (*Johnson et al.*, 1999; *de Baar and de Jong*, 2001; *Moore et al.*, 2004). Fe concentrations in the sediment pore waters are often several orders of magnitude larger than in the seawater. A large part of the iron released to the ocean either by diffusion or by resuspension is likely to be oxidized in insoluble forms and trapped back to the sediments, at least in oxygenated waters (*de Baar and de Jong*, 2001). Yet, some of this iron should escape as observations clearly show increasing concentration gradients of particulate and dissolved iron toward the coastal zones. Unfortunately, almost no quantitative information is available to parameterize this potentially important source.

In a way similar to *Moore et al.* (2004), we apply a maximum constant iron source from the sediments. Since anoxic sediments are more likely to release iron to the seawater, we have modulated this source by a factor computed from the metamodel of *Middelburg et al.* (1996). From this metamodel, it is possible to estimate the relative contribution of anaerobic processes to the total mineralization of organic matter in the sediments, and thus to have an indication on how well the sediment is oxygenated (*Soetaert et al.*, 2000). Our modulation factor is simply set equal to this relative contribution. The maximum iron flux from the sediments has been set to 1 μmol Fe/m^2/d by crudely adjusting the modeled iron distribution to the few iron

observations available over the continental margins. This value is close to that used by *Moore et al.* (2004) in their model (2 μmol Fe/m²/d).

Unfortunately, due to the coarse resolution of ORCA2, the model bathymetry is not able to correctly represent the critical spatial scales of the ocean bathymetry. An example is the continental shelves, which typically have a width scale of 10-30 km, which can be approximately an order of magnitude less than the horizontal resolution of the model. In order to take sub-model gridscale bathymetric variations into account in the Fe source function, the model grid structure has been compared with the high-resolution ETOPO5 dataset. An algorithm was developed whereby for each and every horizontal grid cell, the corresponding region in the ETOPO5 dataset is considered. For each vertical level in the model corresponding to a particular horizontal gridpoint, the corresponding ocean bottom area from ETOPO5 (in fractional units) is saved, with the end result being a three dimensional array containing an equivalent area for the bottom bathymetry of the ocean for the ETOPO5 dataset. The iron flux computed as described above is then multiplied by this fractional area.

For all nutrients except iron and nitrogen, as well as DIC and Alkalinity, the external sources are exactly balanced by an equivalent loss from the bottom of the ocean. This loss is made proportional to the sinking rate and is assumed to represent geological burial within the sediments. For nitrogen, this loss is set equal to atmospheric deposition and riverine input since nitrogen fixation is hypothesized to compensate for denitrification. For iron, all the particulate iron that reaches the bottom of the ocean is definitely removed from the ocean.

Table 1: Model coefficients with their standard values in
PISCES

Parameter	Units	Value	Description
Phytoplankton			
a	day^{-1}	0.66	Growth rate at 0°C
b	–	1.066	Temperature sensitivity of growth
c	^{deg}C	1	Temperature dependence of growth
α	$(W\,m^{-2})^{-1}\,d^{-1}$	4	initial slope of P-I curve
δ	–	0.05,0.05	exudation of DOC
K_{po_4}	$\mu mol\,P\,l^{-1}$	0.0008,0.004	Half-saturation constant for phosphate
K_{nh_4}	$\mu mol\,N\,l^{-1}$	0.013,0.065	Half-saturation constant for ammonium
K_{no_3}	$\mu mol\,N\,l^{-1}$	1.3,0.26	Half-saturation constant for nitrate
K_{si}^{D}	$\mu mol\,Si\,l^{-1}$	2	Half saturation constant for silicate
K_{Fe}^{min}	$nmol\,Fe\,l^{-1}$	0.02,0.1	Minimum half-saturation constant for iron
K_{Fe}^{max}	$nmol\,Fe\,l^{-1}$	0.08,0.4	Maximum half-saturation constant for iron
P_{max}	$\mu mol\,C\,l^{-1}$	1	Maximum concentration of small nanophytoplankton
D_{max}	$\mu mol\,C\,l^{-1}$	0.5	Maximum concentration of small diatoms
m_P	d^{-1}	0.01	phytoplankton mortality rate
w_P	$d^{-1}\,molC^{-1}$	0.01	Quadratic mortality of phytoplankton
w_P^{max}	$d^{-1}\,molC^{-1}$	0.02	Maximum quadratic mortality of diatoms
K_P	$\mu mol\,C\,l^{-1}$	0.1	Half-saturation constant for mortality
$\theta_{chl,max}$	$mg\,Chl\,mg\,C^{-1}$	0.033,0.05	Maximum Chl/C ratios of phytoplankton
$\theta_{fe,max}$	$\mu mol\,Fe\,mol\,C^{-1}$	10,15	Maximum Fe/C ratios of phytoplankton
K_{Si}^{2}	$\mu mol\,Si\,l^{-1}$	5	Half saturation constant for Si/C increase
Zooplankton			
			Table 1 – continued on next page

Table 1 – continued from previous page

Parameter	Units	Value	Description
ϵ	–	0.35,0.35	Zooplankton growth efficiency
σ	–	0.3,0.3	Fecal pellets production
g	d^{-1}	4,0.7	Maximum grazing rate
g_{FF}^M	$(m\,mol\,l^{-1})^{-1}$	$5\,10^3$	Maximum flux feeding rate
K_G	$\mu mol\,C\,l^{-1}$	20,20	Half-saturation constant for grazing
p_P^Z,γ_P	–	0.5,0.2	Preferences for nanophytoplankton
p_D^Z,γ_D	–	0.5,1	Preferences for diatoms
$\mathrm{p}_{POC}^Z,\gamma_{POC}$	–	0.,0.2	Preferences for POC$_s$
γ_Z	–	1.	Preference for microzooplankton
P_{min}	$\mu mol\,C\,l^{-1}$	0.1	Minimum available concentration of nanophytoplankton
m^M	$(\mu mol C\,l^{-1})^{-1}d^{-1}$	0.03	Mesozooplankton mortality
r	d^{-1}	0.03,0.008	Excretion rate
K	$\mu mol\,C\,l^{-1}$	0.1	Half-saturation constant for excretion
ϵ	-	0.5,0.5	
$\left(\frac{Fe}{C}\right)^{zoo}$	$\mu mol\,Fe\,mol C^{-1}$	3	Fe/C ratio of zooplankton
Organic matter			
λ_{DOC}	d^{-1}	0.3	Remineralization rate of DOC
K_{DOC}^{bac}	$\mu mol C\,l^{-1}$	417	Half-saturation constant for DOC remin.
λ_{POC}	d^{-1}	0.025	Degradation rate of POC
w_{min}	$m\,d^{-1}$	3,50	Minimum sinking speed of POC
w_{max}	$m\,d^{-1}$	200	Maximum sinking speed of POC$_b$
$\Phi_1^{DOC},\Phi_2^{DOC}$	$(mol\,C\,l^{-1})^{-1}$	80,698	Aggregation rates for DOC $\rightarrow$ POC$_s$
Φ_3^{DOC}	$(mol\,C\,l^{-1})^{-1}$	10500	Aggregation rates for DOC $\rightarrow$ POC$_b$
$\Phi_1^{POC_s},\Phi_2^{POC_s}$	$(mol\,C\,l^{-1})^{-1}$	940,10540	Aggregation rates for POC$_s$ $\rightarrow$ POC$_b$
$\Phi_3^{POC_s},\Phi_4^{POC_s}$	$(mol\,C\,l^{-1})^{-1}$	0.66,0	Aggregation rates for POC$_s$ $\rightarrow$ POC$_b$
λ_{Fe}^{min}	d^{-1}	$3 10^{-5}$	scavenging rate of iron
λ_{Fe}	$d^{-1}\,\mu mol^{-1}\,l$	0.004	scavenging rate of iron
λ_{CaCO3}	d^{-1}	0.03	Dissolution rate of calcite
λ_{BSi}	d^{-1}	0.015	Dissolution rate of BSi
λ_{NH_4}	d^{-1}	0.05	Maximum nitrification rate
O_2^{min}	$\mu mol O_2\,l^{-1}$	1	Half saturation constant for denitrification
Stoichiometric ratios			
R_{NO3}	$mol\,C\,mol\,N^{-1}$	-0.8	C/N ratio of denitrification
R_{CaCO3}	–	0.4	Maximum rain ratio

4 Model structure

The model is being coded in mixed FORTRAN 77/90. Even if very few capabilities of the Fortran 90 are used, it will not compile with a F77-only compiler (like the gnu g77 compiler). To activate PISCES, the cpp key key_trc_pisces should be declared. The biogeochemical code does not include any other cpp keys.

Only the subroutines that compute the biological or chemical sources and sinks are considered to be part of PISCES. Thus, this excludes the computation of the advection-diffusion equation (the transport of the tracers), as it is not specific to PISCES. There are two types

of subroutines: The initialization of the tracers and of the parameters and the computation of the various biogeochemical sources and sinks. The latter PISCES subroutines are called from within the ocean model timeloop. There is no need for them to be called at the same frequency than the computation of the advection-diffusion terms or of the dynamics. However, the biological time step should be small enough, typically one hour, to avoid major instabilities, which occur when the sources and sinks become larger than the tracer concentrations. Such instabilities could be avoided by the use of an implicit scheme, which is not implemented yet.

The objective here is not to precisely detail the PISCES code but rather to list the different subroutines and to briefly describe their role. All the subroutines that compute the biogeochemical sources/sinks are called from p4zprg which is then the main PISCES subroutine.

p4zbio.F: Computation of the new tracer concentrations by summing up all the different sources and sinks.

p4zche.F: Computation of the various chemical constants.

p4zday.F: Computation of the day length.

p4zdiat.F: Computation of the mortality terms of diatoms.

p4zflx.F: Air-sea fluxes of CO2 and O2.

p4zint.F: Time interpolation of various terms (dust deposition, growth rate, ...).

p4zlim.F: Co-limitations by the different nutrients.

p4zlys.F: Calcite dissolution

p4zmeso.F: Sources and sinks of mesozooplankton (mortality, grazing, ...)

p4zmicro.F: Sources and sinks of microzooplankton.

p4znano.F: Computation of the various mortality terms of nanophytoplankton.

p4zopt.F: Optical model and computation of the euphotic depth.

p4zprod.F: Growth rate of the two phytoplankton groups.

p4zrem.F: Remineralization of organic matter, dissolution of biogenic silica, scavenging.

p4zsed.F: Top and bottom boundary conditions of the biogeochemical tracers (deposition, sedimentary losses, ...).

p4zsink.F: Aggregation of organic matter, computation of the particles sinking speeds.

p4zsink2.F: Sinking of the various particle compartments, based on the MUSCL advection scheme.

Besides the subroutines listed above, several subroutines perform the model initialization. We will only discuss the initialization of the parameters necessary to PISCES. The tracers concentrations are excluded here as their initialization highly depends on the ocean model. Of course, all the initializing subroutines are called only once at the beginning of the simulation.

trclsm.F, trclsm.pisces.h: Reading of the namelist which sets the biological parameters.

trcini.F, trcini.pisces.h: Reading of the boundary conditions (dust deposition, sediment mobilization, ...), initialization of various biogeochemical parameters.

PISCES requires specific dynamical variables to work properly. Thus, if a coupling with a new dynamical model is undertaken, the following dynamical parameters should be absolutely passed to PISCES: Temperature, salinity, mixed layer depth, sea ice concentration, short wave radiation at the ocean surface, wind speed (or at least, wind stress).

In this document, all the model equations and parameterizations adopted in PISCES have been described. Of course, the notation chosen to write in these equations is not identical to that of the Fortran code. To ease the manipulation of the code and of the namelist, Table 2 displays the translation between the equation and the code notations for the parameters of the namelist (thus, those that can be changed without recompiling the model). Table 3 lists all the model tracers and their indices in the code.

Table 2: Translation between the FORTRAN code and
the model equations

Equation name	Code name	Description
	Phytoplankton	
α	pislope, pislope2	Initial slope of the PI curve
δ	excret	Excretion of DOC
K_{po_4}	concnnh4, concdnh4	Half-saturation constant for Phosphate
K_{nh_4}	concnnh4, concdnh4	Half-saturation constant for ammonium
K_{no_3}	conc0, conc1	Half-saturation constant for nitrate
K_{si}^D	xksi1	Half saturation constant for silicate
K_{Fe}^{min}	conc2, conc3	Minimum half-saturation constant for iron
m_P	mprat, mprat2	phytoplankton mortality rate
w_P	wchl	Quadratic mortality of phytoplankton
w_P^{max}	wchld	Maximum quadratic mortality of diatoms
K_P	xkmort	Half-saturation constant for mortality
$\theta_{chl,max}$	chlcnm, chlcdm	Maximum Chl/C ratios of phytoplankton
$\theta_{fe,max}$	fecnm, fecdm	Maximum Fe/C ratios of phytoplankton
K_{Si}^2	xksi2	Half saturation constant for Si/C increase
	Zooplankton	
ϵ	epsher, epsher2	Zooplankton growth efficiency
σ	sigma1, sigma2	Fecal pellets production
g	grazrat, grazrat2	Maximum grazing rate
K_G	xkgraz, xkgraz2	Half-saturation constant for grazing
p_P^Z, γ_P	zprefp, xprefp	Preferences for nanophytoplankton
p_D^Z, γ_D	zprefd, xprefd	Preferences for diatoms
p_{POC}^Z, γ_{POC}	zprefc, xprefpoc	Preferences for POC_s
γ_Z	xprefz	Preference for microzooplankton
m^M	mzrat2	Mesozooplankton mortality
r	resrat, resrat2	Excretion rate
K	xkmort	Half-saturation constant for excretion
$\left(\frac{Fe}{C}\right)^{zoo}$	ferat3	Fe/C ratio of zooplankton
		Table 2 – continued on next page

17

Table 2 – continued from previous page

Equation name	Code name	Description
Organic matter		
λ_{DOC}	xremik	Remineralization rate of DOC
K_{DOC}^{bac}	xkdoc	Half-saturation constant for DOC remin.
λ_{POC}	xremip	Degradation rate of POC
w_{min}	wsbio, wsbio2	Minimum sinking speed of POC
λ_{Fe}	xlam1	scavenging rate of iron
λ_{BSi}	xsirem	Dissolution rate of BSi
λ_{NH_4}	nitrif	Maximum nitrification rate
O_2^{min}	oxymin	Half saturation constant for denitrification
Stoichiometric ratios		
R_{CaCO3}	caco3r	Maximum rain ratio

Table 3: Description of the model indices

PISCES indices	Units	Description
jpdic	$mol\,C\,l^{-1}$	Dissolved inorganic carbon
jptal	$eq\,l^{-1}$	Total alkalinity
jpoxy	$mol\,O_2\,l^{-1}$	dissolved oxygen
jpcal	$mol\,C\,l^{-1}$	Calcite
jppo4	$mol\,C\,l^{-1}$	Phosphate
jppoc	$mol\,C\,l^{-1}$	Small particulate organic carbon
jpsil	$mol\,Si\,l^{-1}$	silicate
jpphy	$mol\,C\,l^{-1}$	Nanophytoplankton
jpzoo	$mol\,C\,l^{-1}$	Microzooplankton
jpdoc	$mol\,C\,l^{-1}$	Semi-labile dissolved organic carbon
jpdia	$mol\,C\,l^{-1}$	Diatoms
jpmes	$mol\,C\,l^{-1}$	Mesozooplankton
jpbsi	$mol\,Si\,l^{-1}$	Silicon content of the diatoms
jpfer	$mol\,Fe\,l^{-1}$	Dissolved iron
jpbfe	$mol\,Fe\,l^{-1}$	Iron in the big particles
jpgoc	$mol\,C\,l^{-1}$	Big particulate organic carbon
jpsfe	$mol\,Fe\,l^{-1}$	Iron in the small particles
jpdfe	$mol\,Fe\,l^{-1}$	Iron content of the diatoms
jpdsi	$mol\,Si\,l^{-1}$	Sinking biogenic silica
jpnfe	$mol\,Fe\,l^{-1}$	Iron content of the nanophytoplankton
jpnch	$kg\,Chl\,l^{-1}$	Chlorophyll of the nanophytoplankton
jpdch	$kg\,Chl\,l^{-1}$	Chlorophyll of the diatoms
jpno3	$mol\,C\,l^{-1}$	Nitrate
jpnh4	$mol\,C\,l^{-1}$	Ammonium

5   Atlas of model results

In this section, model results are compared to available observations. Rather than commenting out all the figures, we present here an atlas and let the figures speak by themselves. Some discussion on the model results can be found in several publications which have been published and which should appear soon in the literature. The reader could refer to these references for more information (*Aumont and Bopp*, 2005; *Bopp et al.*, 2005; *Gehlen et al.*, 2005; *Raynaud et al.*, 2005).

References

Alvain, S., C. Moulin, Y. Dandonneau, and F.-M. Bréon (2005), Remote sensing of phytoplankton groups in case 1 waters from global SeaWiFS imagery, *Deep Sea Res. Part I*, in press.

Armstrong, R. A. (1994), Grazing limitation and nutrient limitation in marine ecosystems: Steady-state solutions of an ecosystem model with multiple food chains, *Limnol. Oceanogr.*, *39*, 597–608.

Armstrong, R. A., C. Lee, J. I. Hedges, S. Honjo, and S. G. Wakeham (2002), A new, mechanistic model for organic carbon fluxes in the ocean based on the quantitative association of POC with ballast minarals, *Deep Sea Res. Part II*, *49*, 219–236.

Aumont, O. (1998), Etude du cycle naturel du carbone dans un modèle 3D de l'océan mondial, Ph.D. thesis, Univ. Paris VI, Paris.

Aumont, O., and L. Bopp (2005), Globalizing results from ocean in-situ iron fertilization studies, *Global Biogeochem. Cycles*, accepted.

Aumont, O., S. Belviso, and P. Monfray (2002), Dimethylsulfoniopropionate (dmsp) and dimethylsulfide (dms) sea surface distributions simulated from a global 3-d ocean carbon cycle model, *J. Geophys. Res.*, *107*, doi:10.1029/1999JC000111.

Aumont, O., E. Maier-Reimer, S. Blain, and P. Monfray (2003), An ecosystem model of the global ocean including Fe, Si, P co-limitation, *Global Biogeochem. Cycles*, *17*, 1060, doi: 10.1029/2001GB001745.

Berelson, W. M. (2002), Particle settling rates increase with depth in the ocean, *Deep Sea Res. Part II*, *49*, 237–251.

Bonnet, S., and C. Guieu (2004), Dissolution of atmospheric iron in seawater, *Geophys. Res. Lett.*, *31*, L03303, doi:10.1029/2003GL018423.

Bopp, L., O. Aumont, P. Cadule, S. Alvain, and M. Gehlen (2005), Response of diatoms distribution to global warming and potential implications: A global model study, *Geophys. Res. Lett.*, *32*, L19606, doi:10.1029/2005GL023653.

Brzezinski, M. A., and D. M. Nelson (1988), Differential cell sinking as a factor influencing diatom species competition for limiting nutrient, *Journal of Experimental Marine Biology and Ecology*, *119*, 179–200.

Buitenhuis, E., C. Le Quéré, O. Aumont, A. Bunker, A. Hirst, T. Ikeda, T. O'Brien, S. Pontkiovski, and D. Straile (2005), Biogeochemical fluxes through mesozooplankton, *Global Biogeochem. Cycles*, submitted.

Chen, M., and W.-X. Wang (2001), Bioavailability of natural colloidal-bound iron to marine phytoplankton: Influences of colloidal size and aging, *Limnol. Oceanogr.*, *46*, 1956–1967.

Chen, M., R. C. H. Dei, W.-X. Wang, and L. Guo (2003), Marine diatom uptake of iron bound with natural colloids of different origins, *Marine Chemistry*, *81*, 177–189.

Claquin, P., V. Martin-Jézéquel, J. C. Kromkamp, M. Veldhuis, and G. Kraay (2002), Uncoupling of silicon compared to carbon and nitrogen metabolism, and the role of the cell cycle, in continuous cultures of *Thalassiosira Pseudonana* (Bacillariophyceae), under light, nitrogen, and phosphorus control, *Journal of Phycology*, *38*, 922–930.
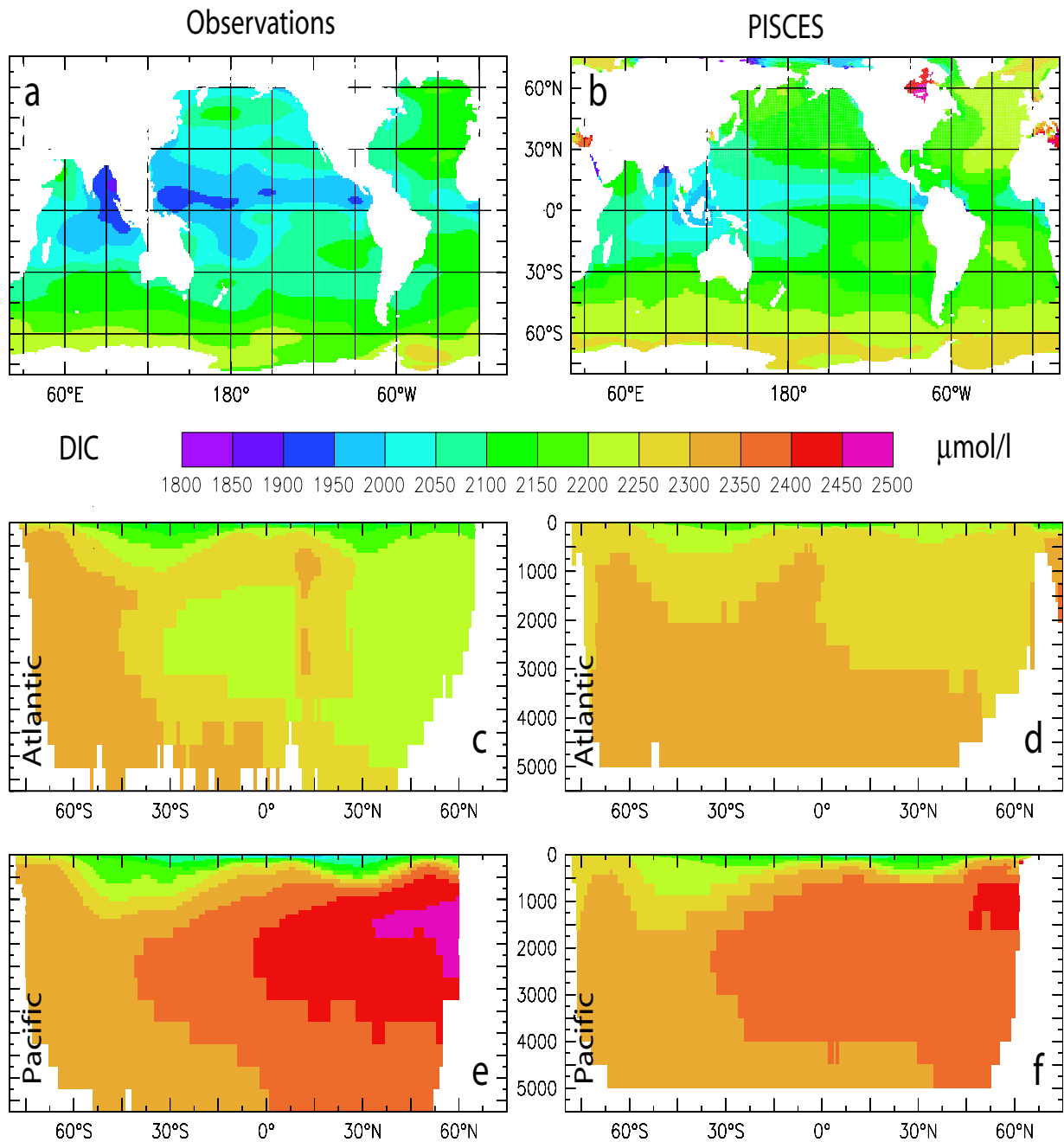
Figure 2: Annual mean DIC concentrations in μmol kg^{-1}. Observations are from GLODAP. (a) Observed surface. (b) Model run surface. (c) Observed transect zonally averaged over the Atlantic. (d) Same as (c) but for the model. (e) Observed transect zonally averaged over the Pacific. (f) Same as (e) but for the model.
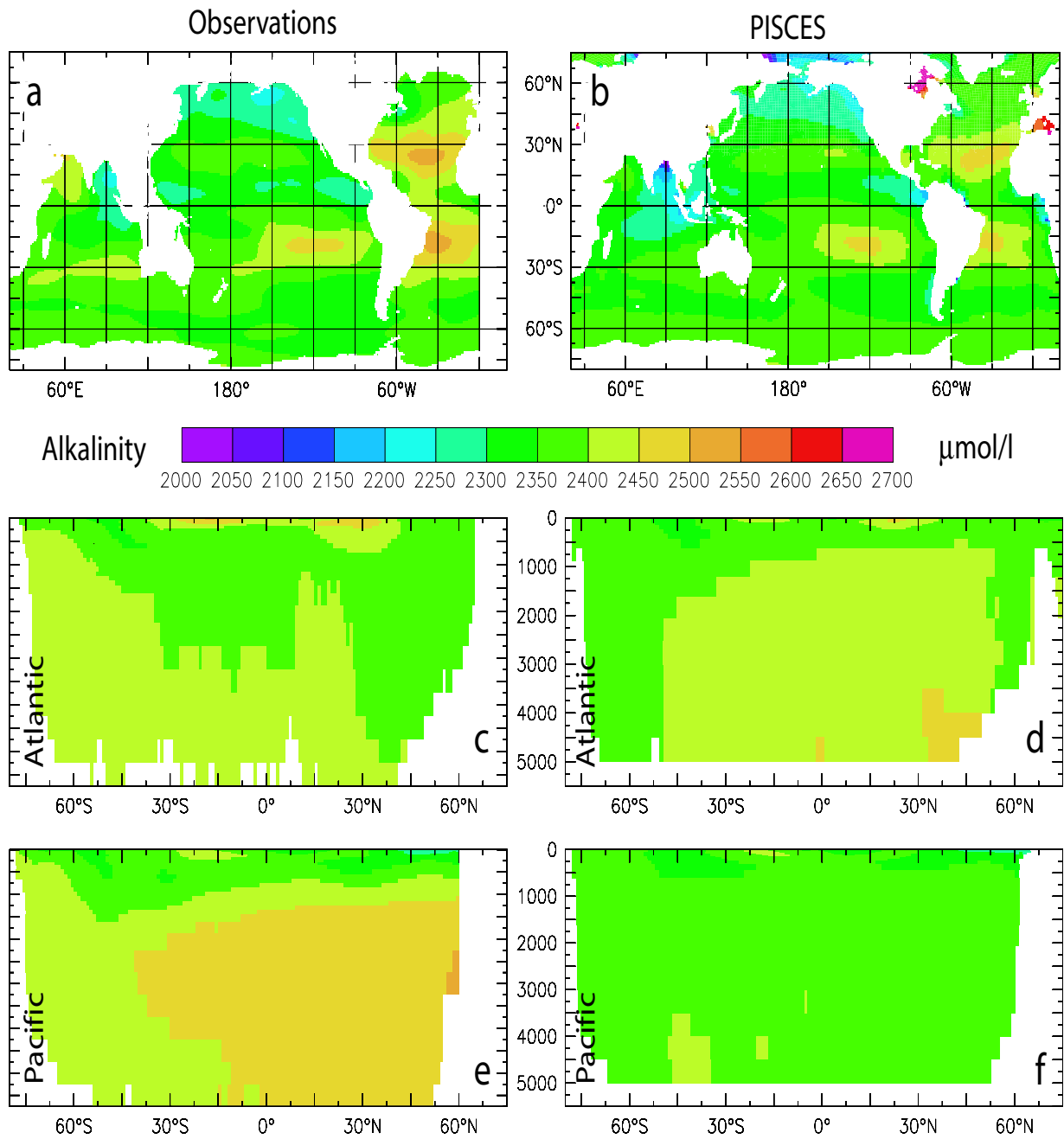
Figure 3: Annual mean Alkalinity concentrations in μeq kg^{-1}. Observations are from GLODAP. Panels are the same as on Figure 2
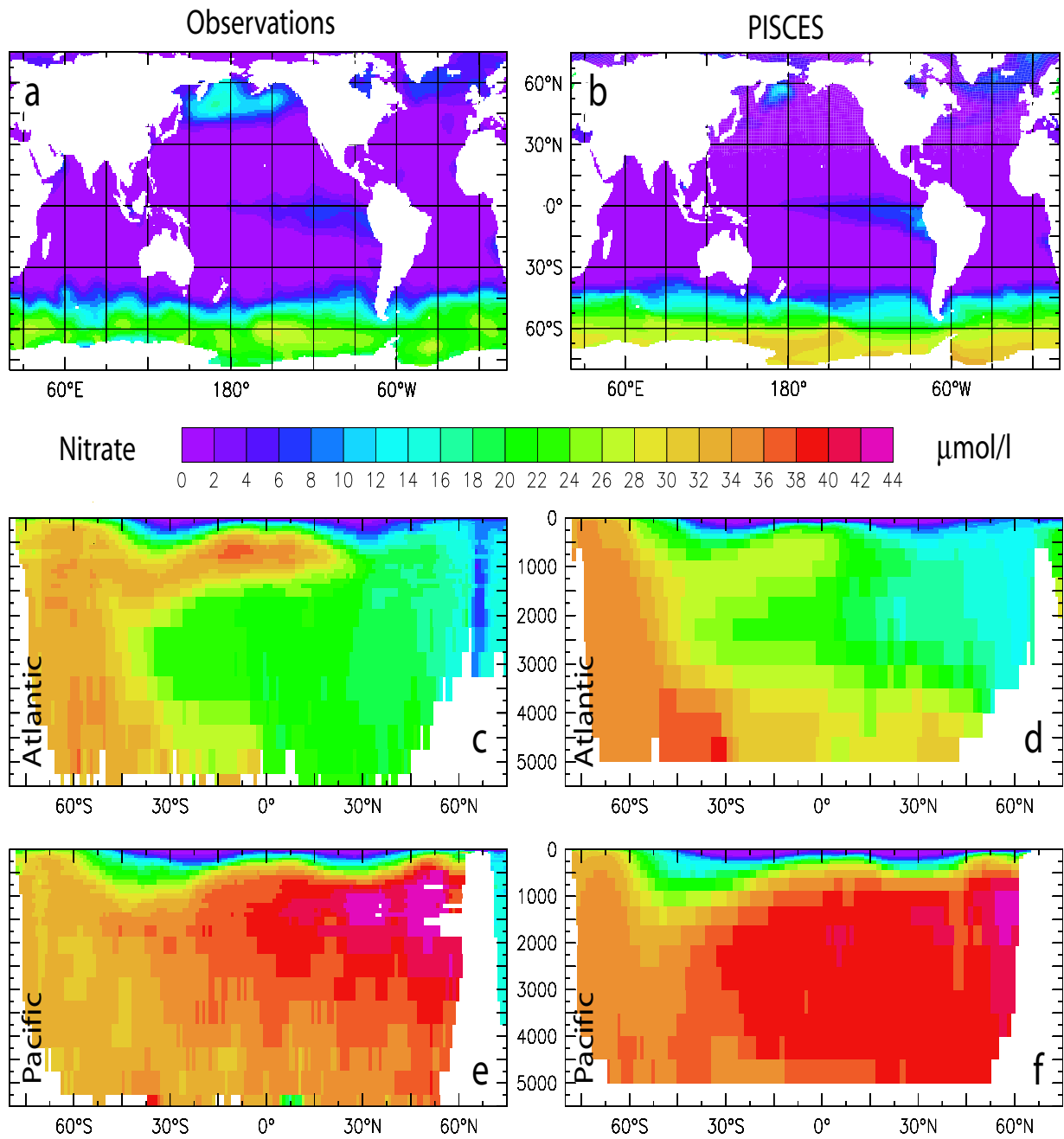
Figure 4: Annual mean nitrate concentrations in $\mu\mathrm{mol\,L}^{-1}$. Observations are from the World Ocean Atlas 2001. Panels are the same as on Figure 2
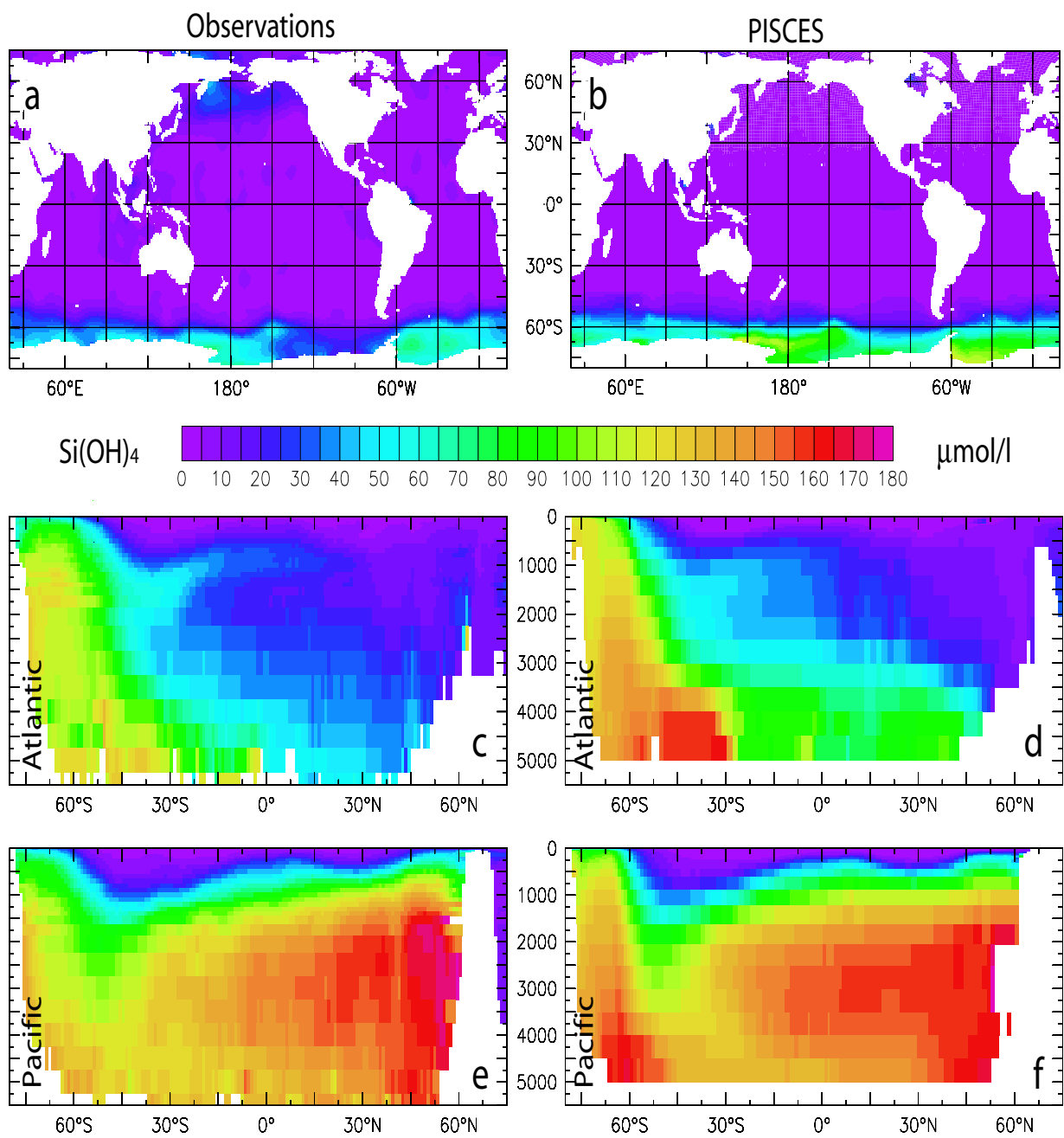
Figure 5: Annual mean silicate concentrations in $\mu mol\, L^{-1}$. Observations are from the World Ocean Atlas 2001. Panels are the same as on Figure 2
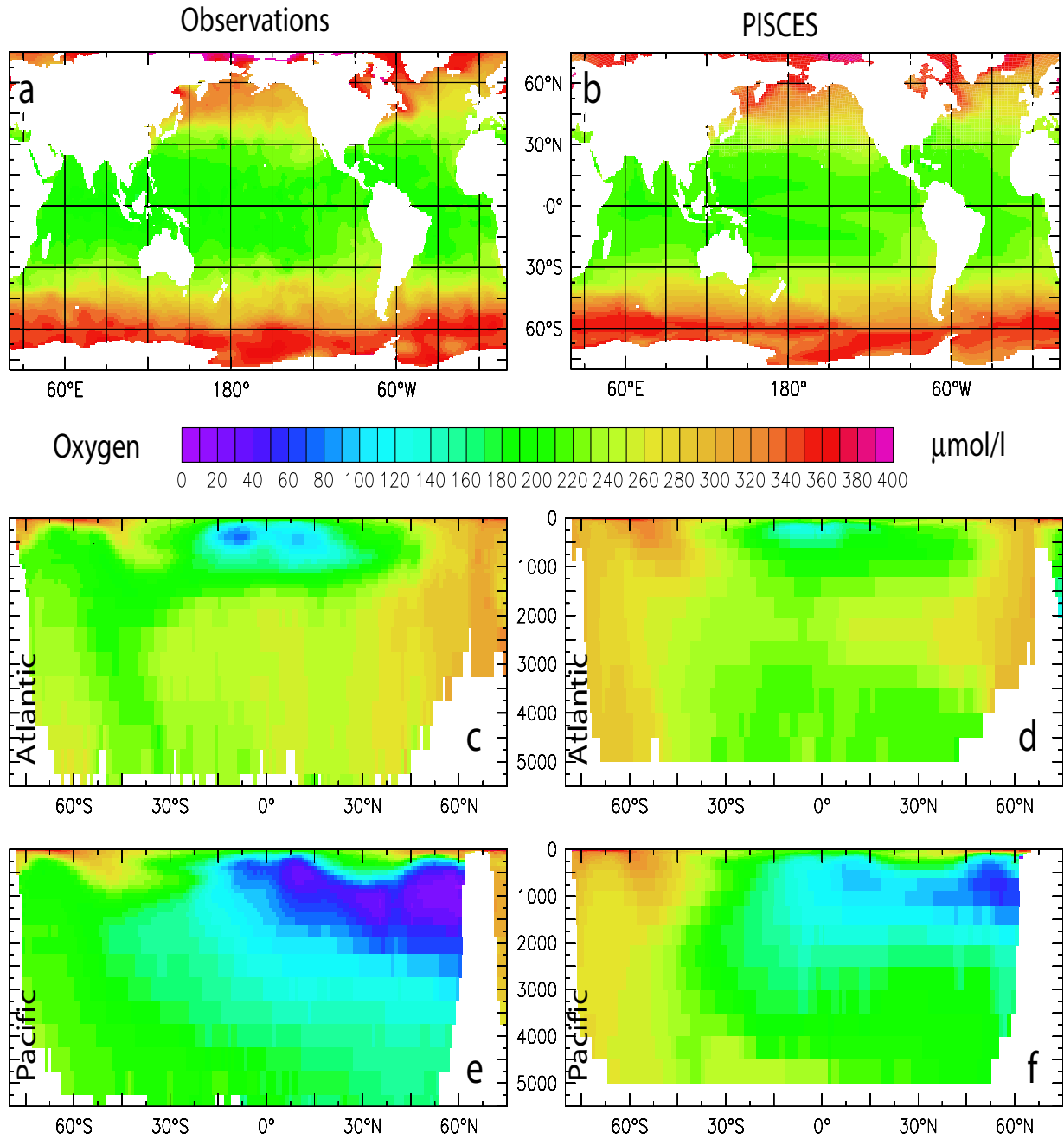
Figure 6: Annual mean oxygen concentrations in μmol L^{-1}. Observations are from the World Ocean Atlas 2001. Panels are the same as on Figure 2

a   Surface

b   1000 m depth

Dissolved Fe Concentrations (nM)

0   0.1   0.2   0.3   0.4   0.5   0.6   0.7   0.8   0.9   1   2   3   4   5
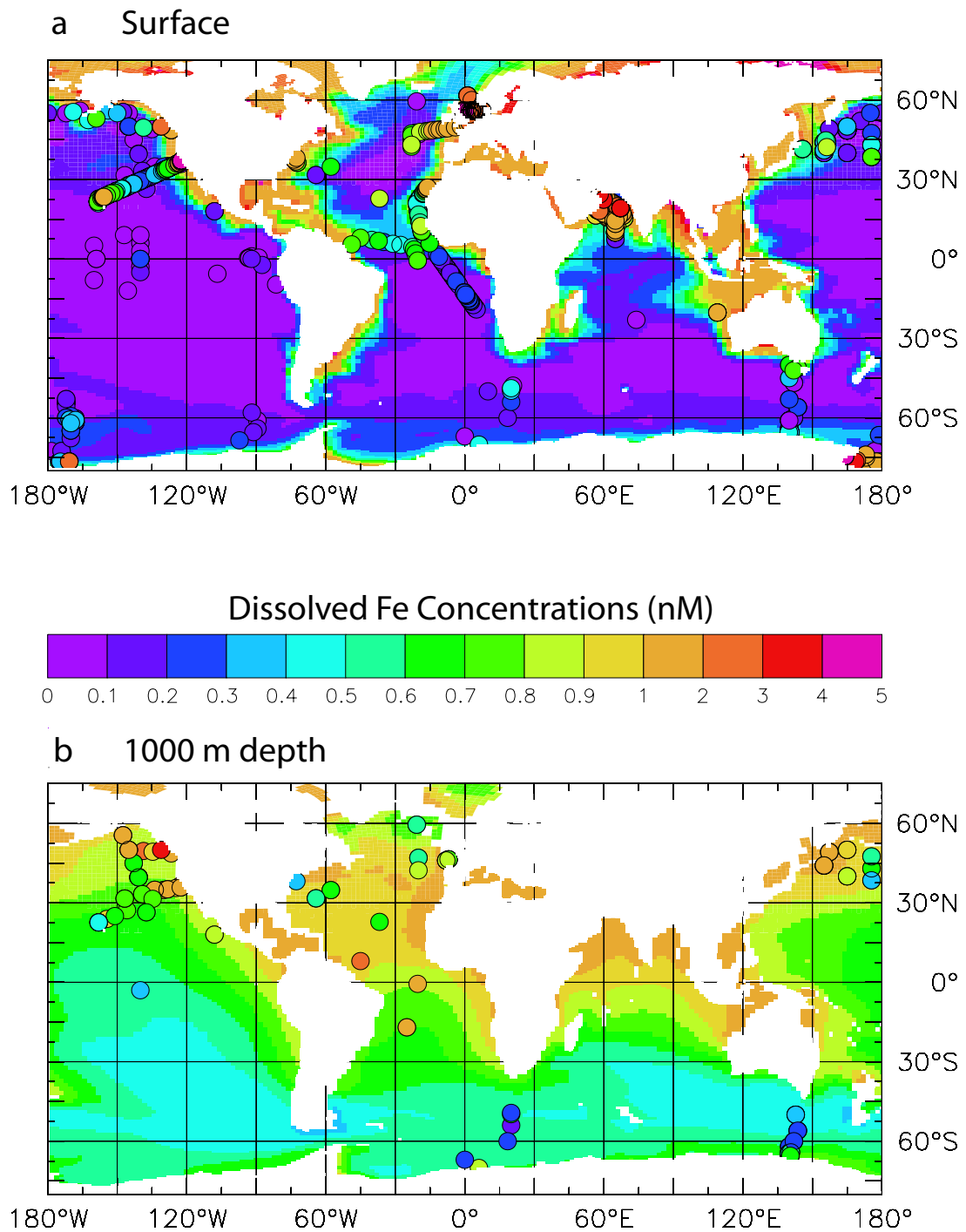
Figure 7: Comparison to observations: Dissolved iron (in nM) from PISCES, annual mean, (a) at the surface, and (b) at 1000 m depth. Available observations, mainly based on *Gregg et al.* (2003) and *Parekh et al.* (2004) compilations are displayed as dots but with the same color code.
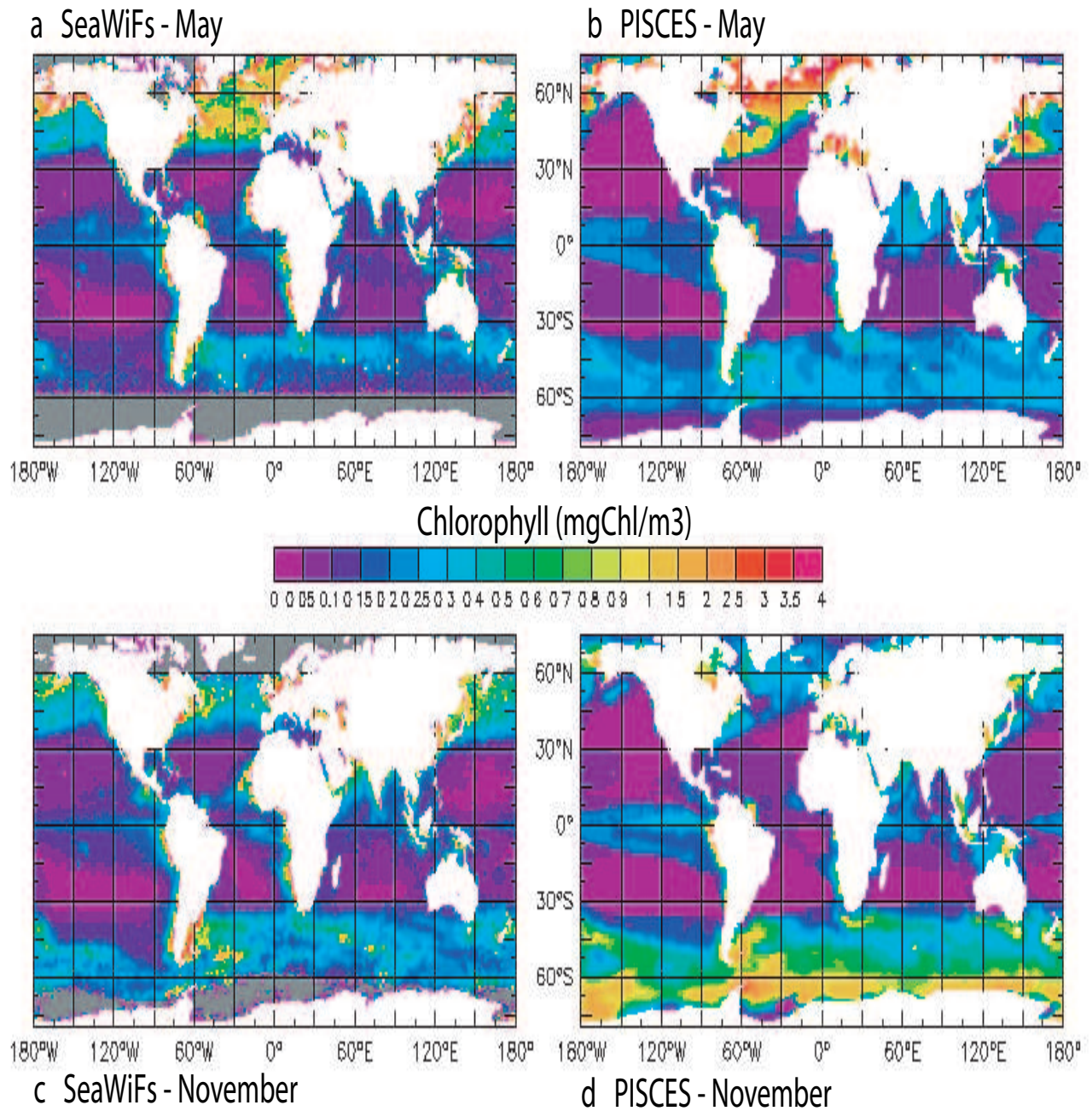
Figure 8: Comparison to observations: Surface chlorophyll (in $\mathrm{mg\,m^{-3}}$) derived from remote sensing (SeaWiFS) over 1997-2003 for (a) May and (b) November, compared to simulated chlorophyll from PISCES (c) May, and (d) November. The grey shaded areas on panels (a) and (c) denote the lack of observations.

27

a PHYSAT

Diatoms Index (Relative Unit)

b PISCES
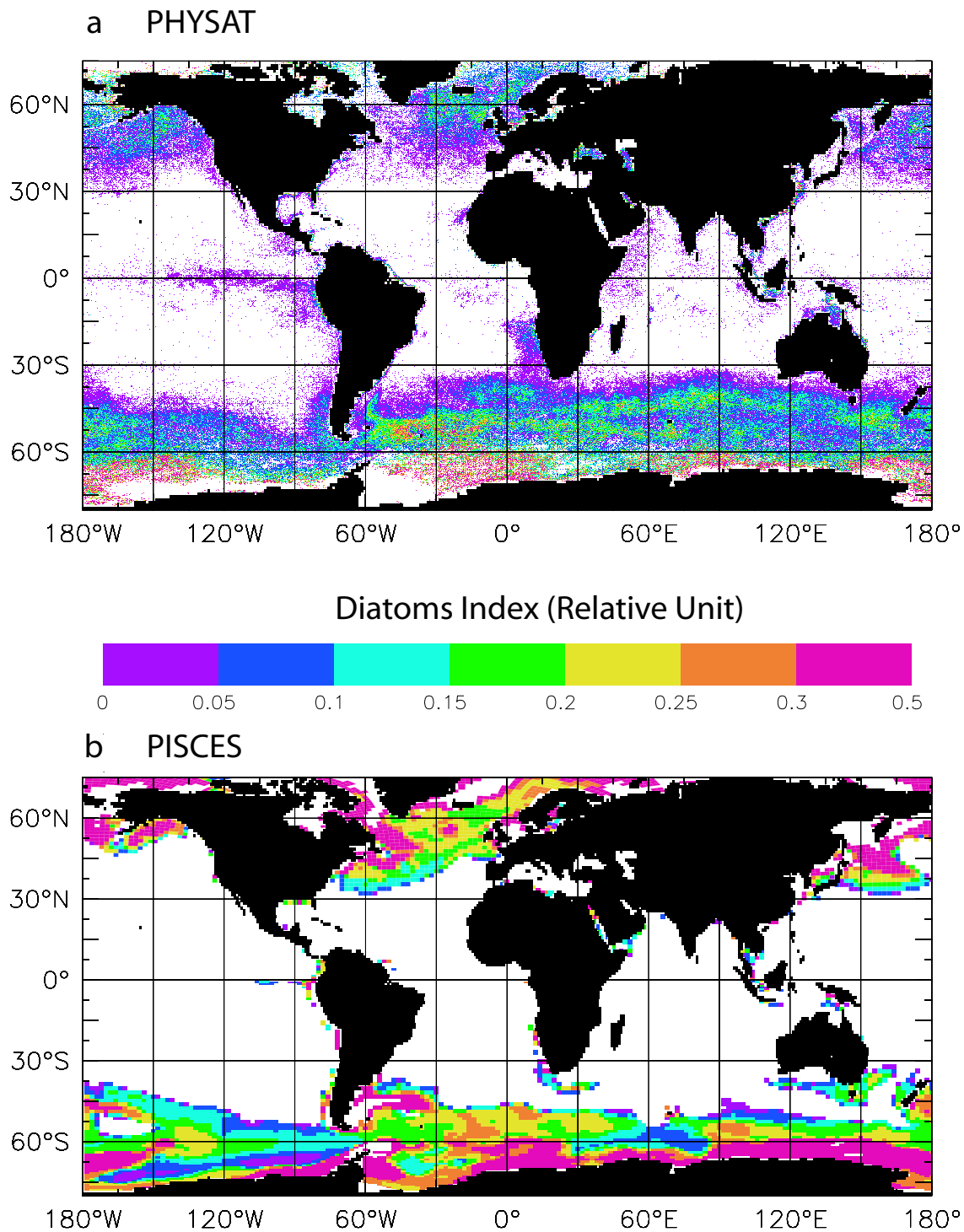
Figure 9: Climatological PHYSAT and simulated distributions of a diatoms index. The diatoms index represents the relative time in a year when diatoms are blooming: we divide the number of days when diatoms are blooming by the total number of days in a year. (a) PHYSAT directly diagnoses diatoms blooms (*Alvain et al.*, 2005). (b) Diatoms are considered as blooming in the model when $[Chl] > 0.5$ mgChl m^{-3} and diatoms relative abundance > 45%.
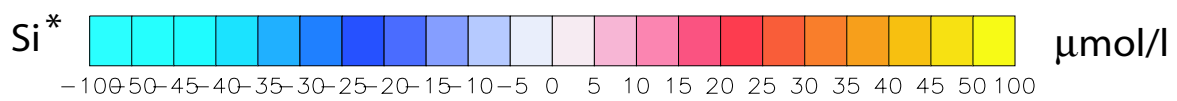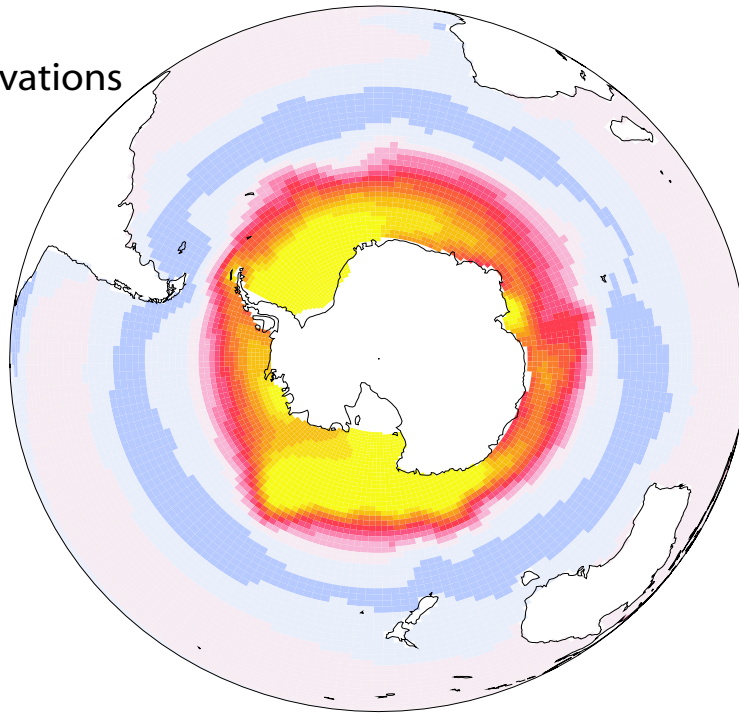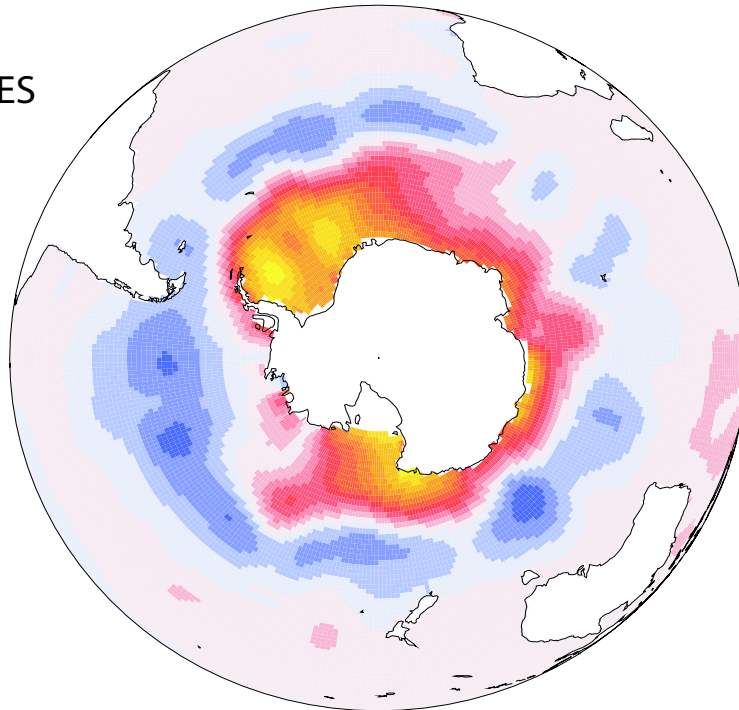
Figure 10: Polar stereographic map of sea-surface Si* (see *Sarmiento et al.* (2004) for the definition of this tracer) (a) from the observations and (b) from the model. Concentrations in μmol L^{-1} are annually averaged.
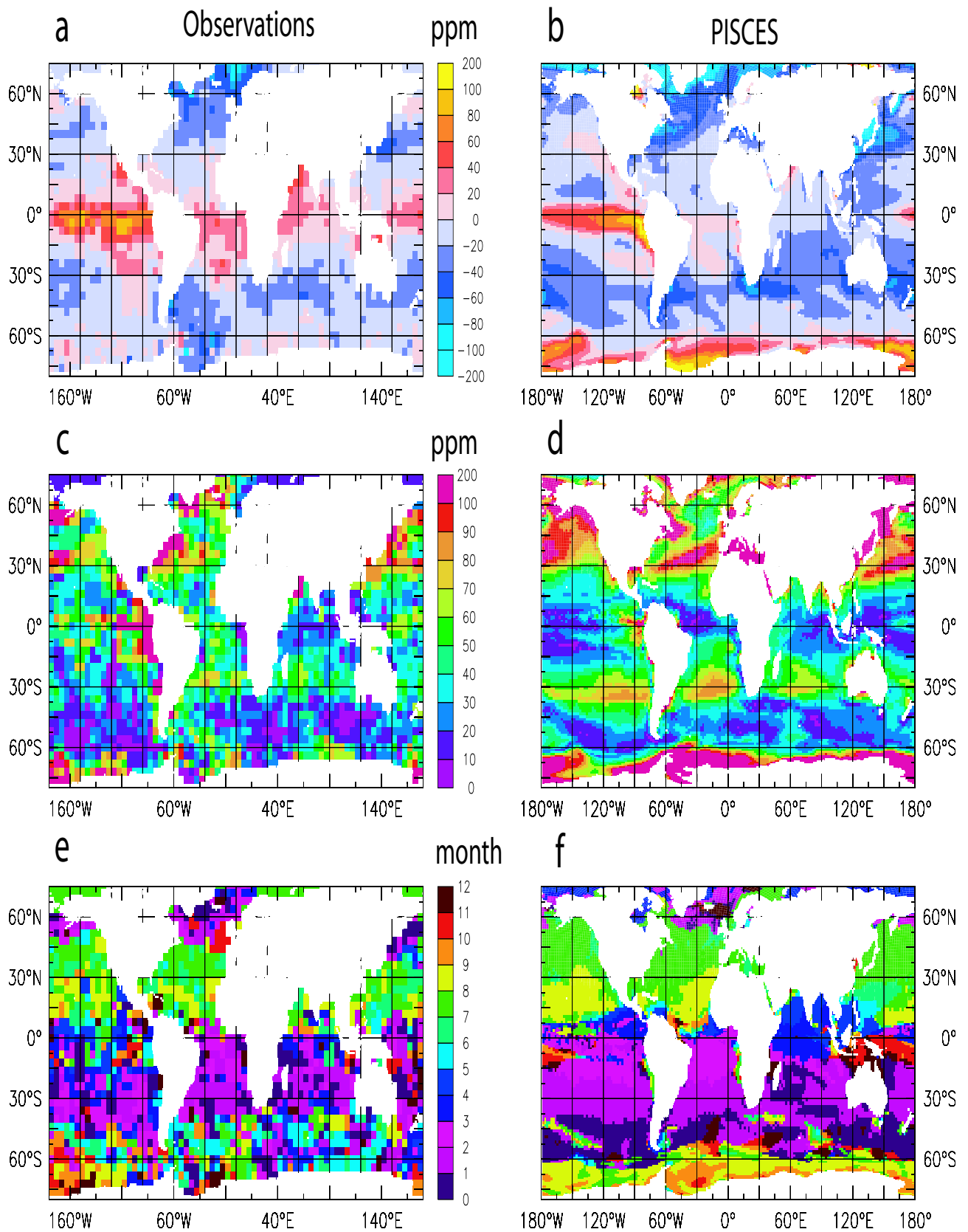
Figure 11: Comparison of modeled surface ΔpCO_2 to observations from *Takahashi et al.* (1997). (a) and (b) Annual mean surface ΔpCO_2 in ppmv. (c) and (d) Amplitude of the seasonal cycle in ppmv. This amplitude is defined as the difference between the maximum value and the minimum value reached in the year. (e) and (f) Month during which the maximum value is reached. One corresponds to January and twelve to December.
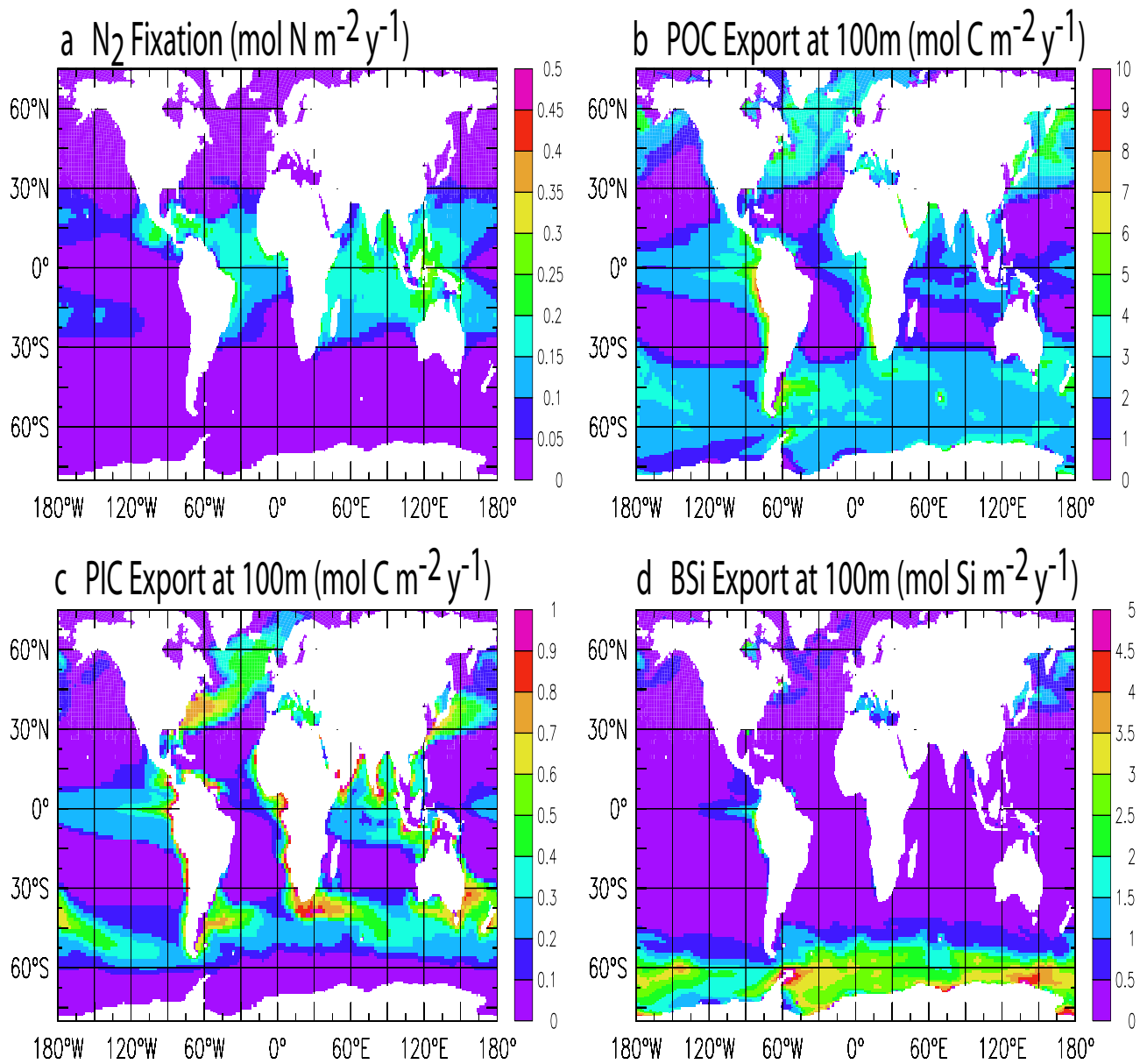
Figure 12: Annual mean fluxes simulated by PISCES. (a) Nitrogen fixation in mol N m^{-2} yr^{-1}. (b) Export of POC at 100m in mol C m^{-2} yr^{-1}. (c) Export of CaCO3 at 100m in mol C m^{-2} yr^{-1}. (d) Export of Biogenic Si at 100m in mol Si m^{-2} yr^{-1}.
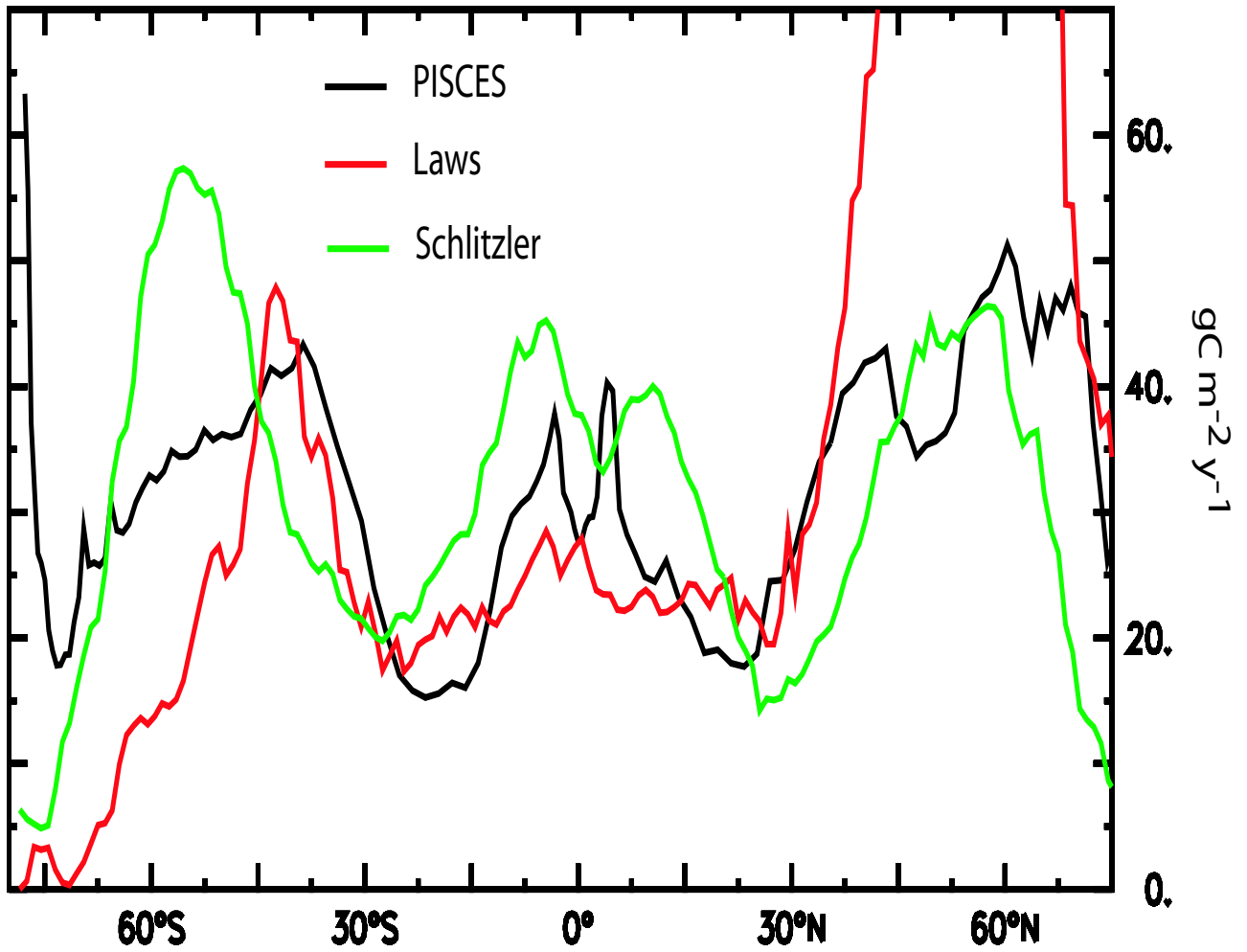
Figure 13: Comparison of zonal mean POC export at 100m predicted by PISCES to various published estimates (*Schlitzer*, 2000; *Laws et al.*, 2000).

de Baar, H. J. W., and J. T. M. de Jong (2001), Distributions, sources and sinks of iron in seawater, in *The biogeochemistry of iron in seawater*, edited by D. Turner and K. Hunter, pp. 85–121, John Wiley, Hoboken, N. J.

Dilling, L., and A. L. Alldredge (2000), Fragmentation of marine snow by swimming macro-zooplankton: A new process impacting carbon cycling in the sea, *Deep Sea Res. Part I*, *47*, 1227–1245.

Donald, K. M., D. J. Scanlan, N. G. Carr, N. H. Mann, and I. Joint (1997), Comparative phosphorus nutrition of the marine cyanobacterium *Synechococus* WH7803 and the marine diatom *Thalassiosira Weissflogii*, *J. of Plankton Res.*, *19*, 1793–1814.

Droop, M. R. (1983), 25 years of algal growth kinetics, *Bot. Mar.*, *26*, 99–112.

Eppley, R. W., J. N. Rogers, and J. J. McCarthy (1969), Half-saturation constants for uptake of nitrate and ammonium by marine phytoplankton, *Limnol. Oceanogr.*, *14*, 912–920.

Fasham, M. J. R., J. L. Sarmiento, R. D. Slater, H. W. Ducklow, and R. Williams (1993), Ecosystem behavior at Bermuda Station "S" and Ocean Weather Station "India": A general circulation model and observational analysis, *Global Biogeochem. Cycles*, *7*, 379–416.

Franck, V. M., M. A. Brzezinski, K. H. Coale, and D. M. Nelson (2000), Iron and silicic acid concentrations regulate Si uptake north and south of the Polar Frontal Zone in the Pacific Sector of the Southern Ocean, *Deep Sea Res. Part II*, *47*, 3315–3338.

Frost, B. W. (1987), Grazing control of phytoplankton stock in the open subarctic Pacific Ocean: A model assessing the role of mesozooplankton, particularly the large calanoid copepodes Neocalanus spp., *Mar. Ecol. Prog. Ser.*, *39*, 49–68.

Fung, I. Y., S. K. Meyn, I. Tegen, S. C. Doney, J. G. John, and K. B. Bishop (2000), Iron supply and demand in the upper ocean, *Global Biogeochem. Cycles*, *14*, 281–295.

Gehlen, M., L. Bopp, N. Emprin, O. Aumont, C. Heinze, I. Kriest, and O. Ragueneau (2005), Reconciling surface ocean productivity, export fluxes and sediment composition in a global biogeochemical ocean model, *Global Biogeochem. Cycles*, submitted.

Geider, R. J., H. L. MacIntyre, and T. M. Kana (1996), A dynamic model of photoadaptation in phytoplankton, *Limnol. Oceanogr.*, *41*, 1–15.

Geider, R. J., H. L. MacIntyre, and T. M. Kana (1998), A dynamic regulatory model of phyto-planktonic acclimation to light, nutrients, and temperature, *Limnol. Oceanogr.*, *43*, 679–694.

Gregg, W., P. Ginoux, P. Schopf, and N. Casey (2003), Phytoplankton and iron: Validation of global three-dimensional ocean biogeochemical model, *Deep Sea Res. Part II*, *50*, 3143–3169.

Honeyman, B., L. Balistrieri, and J. Murray (1988), Oceanic trace metal scavenging and the importance of particule concentration, *Deep Sea Res. Part I*, *35*, 227–246.

Honjo, S. (1996), Fluxes of particles to the interior of the open oceans, in *Particle Flux to the Ocean, SCOPE*, vol. 57, edited by V. Ittekkot, P. Schäfer, S. Honjo, and P. J. Depetris, pp. 91–254, Wiley, New York.

Horrigan, S. G., A. F. Carlucci, and P. M. Williams (1981), Light inhibition of nitrification in sea-surface waters, *Journal of Marine Research*, *39*, 557–565.

Hurtt, G. C., and R. A. Armstrong (1996), A pelagic ecosystem model calibrated with BATS data, *Deep Sea Res.*, *43*, 653–683.

Jansen, H., and D. A. Wolf-Gladrow (2001), Carbonate dissolution in copepod guts: a numerical model, *Mar. Ecol. Prog. Ser.*, *221*, 199–207.

Jickells, T. D., and L. J. Spokes (2001), Atmospheric iron inputs to the oceans, in *The biogeochemistry of iron in seawater*, edited by D. Turner and K. Hunter, pp. 85–121, John Wiley, Hoboken, N. J.

Johnson, K. S., F. P. Chavez, and G. E. Friederich (1999), Continental-shelf sediment as a primary source of iron for coastal phytoplankton, *Nature*, *398*, 697–700.

Kriest, I. (2002), Different parameterizations of marine snow in a 1-D model and their influence on representation of marine snow, nitrogen budget and sedimentation, *Deep Sea Res. Part I*, *49*, 2133–2162.

Laws, E. A., P. G. Falkowski, W. O. S. Jr., H. Ducklow, and J. J. McCarthy (2000), Temperature effects on export production in the open ocean, *Global Biogeochem. Cycles*, *14*, 1231–1246.

Lipschultz, F., S. Wofsy, B. Ward, L. Codispoti, G. Friederich, and J. Elkins (1990), Bacterial transformations of inorganic nitrogen in the oxygen-deficient waters of the eastern tropical South Pacific Ocean, *Deep Sea Res. Part I*, *37*, 1513–1541.

Liu, X., and F. J. Millero (2002), The solubility of iron in seawater, *Marine Chemistry*, *77*, 43–54.

Ludwig, W., J. L. Probst, and S. Kempe (1996), Predicting the oceanic input of organic carbon by continental erosion, *Global Biogeochem. Cycles*, *10*, 23–41.

Madec, G., P. Delecluse, M. Imbard, and C. Lévy (1998), OPA8.1 Ocean general circulation model reference manual, *Notes du pôle de modélisation*, IPSL.

Maier-Reimer, E. (1993), Geochemical cycles in an ocean general circulation model: Preindustrial tracer distributions, *Global Biogeochem. Cycles*, *7*, 645–677.

Maier-Reimer, E., U. Mikolajewicz, and K. Hasselmann (1993), Mean circulation of the Hamburg LSG OGCM and its sensitivity to the thermohaline surface forcing, *J. Phys. Oceanogr.*, *23*, 731–757.

Martin-Jézéquel, V., M. Hildebrand, and M. Brzezinski (2000), Silicon metabolism in diatoms: Implications for growth, *Journal of Phycology*, *36*, 1–20.

McCarthy, J. J. (1980), The kinetics of nutrient utilization, *Can. Bull. Fish. Aquat. Sci.*, *210*, 211–233.

Meybeck, M. (1993), Riverine transport of atmospheric carbon: Sources, global typology and budget, *Water, Air, Soil Pollut.*, *70*, 443–463.

Middelburg, J. J., K. Soetaert, P. M. J. Herman, and C. Heip (1996), Denitrification in marine sediments: a model study, *Global Biogeochem. Cycles*, *10*, 661–673.

Milliman, J. D., P. J. Troy, W. M. Balsch, A. K. Adams, Y.-H. Li, and F. T. Mackenzie (1999), Biologically mediated dissolution of calcium carbonate above the chemical lysocline?, *Deep Sea Res. Part I*, *46*, 1653–1669.

Moloney, C. L., and J. G. Field (1991), The size-based dynamics of plankton food webs. I. A simulation model of carbon and nitrogen flows, *J. Plankton Res.*, *13*, 1003–1038.

Monod, J. (1942), *Recherches sur la croissance des cultures bactériennes*, Hermann, Paris.

Moore, J. K., S. C. Doney, J. A. Kleypas, D. M. Glover, and I. Y. Fung (2002), An intermediate complexity marine ecosystem model for the global domain, *Deep Sea Res. Part II*, *49*, 403–462.

Moore, J. K., S. C. Doney, and K. Lindsay (2004), Upper ocean ecosystem dynamics and iron cycling in a global three-dimensional model, *Global Biogeochem. Cycles*, *18*, GB4028, doi:10.1029/2004GB002220.

Morel, A., and J.-F. Berthon (1989), Surface pigments, algal biomass profiles, and potential production of the euphotic layer: relationships reinvistigated in view of remote sensing applications, *Limnol. Oceanogr.*, *34*, 1545–1562.

Muggli, D. L., M. Lecourt, and P. J. Harrison (1996), Effects of iron and nitrogen source on the sinking rate, physiology and metal composition of an oceanic diatom from the subarctic Pacific, *Mar. Ecol. Prog. Ser.*, *132*, 215–227.

Nishioka, J., and S. Takeda (2000), Change in the concentrations of iron in different size-fractions during growth of the oceanic diatom *Chaetoceros* sp. : Importance of small colloidal iron, *Marine Biology*, *137*, 231–238.

O'Neill, R. V., D. L. Angelis, J. J. Pastor, B. J. Jackson, and W. M. Post (1989), Multiple nutrient limitation in ecological models, *Ecological Modelling*, *46*, 147–163.

Parekh, P., M. J. Follows, and E. A. Boyle (2004), Decoupling of iron and phosphate in the global ocean, *Global Biogeochem. Cycles*, GB002280, doi:10.1029/2004GB002280.

Perry, M. J. (1976), Phosphate utilization by an oceanic diatom in phosphorus-limited chemostat culture and in the oligotrophic waters of the central north Pacific, *Limnol. Oceanogr.*, *21*, 88–107.

Pondaven, P., C. Fravalo, D. Ruiz-Pino, P. Tréguer, B. Quéguiner, and C. Jeandel (1998), Modelling the silica pump in the Permanently Open Ocean Zone of the Southern Ocean, *J. Mar. Systems*, *17*, 587–619.

Raimbault, P., M. Rodier, and I. Taupier-Letage (1988), Size-fraction of phytoplankton in the Ligurian Sea and the Algerian Basin (Mediterranean Sea): Size distribution versus total concentration, *Marine Microbial Food Web*, *3*, 1–7.

Raynaud, S., O. Aumont, K. B. Rodgers, P. Yiou, and J. C. Orr (2005), Interannual-to-decadal variability of North Atlantic air-sea CO2, *Ocean Science*, in revision.

Ridgwell, A. J., A. J. Watson, and D. E. Archer (2002), Modelling the response of the oceanic Si inventory to perturbations and consequences for atmospheric CO_2, *Global Biogeochem. Cycles*, *16*, 1071, doi:10.1029/2002GB001877.

Sarmiento, J. L., N. Gruber, M. A. Brzezinski, and J. P. Dunne (2004), High-latitude controls of thermocline nutrients and low latitude biological productivity, *Nature*, *427*, 56–60.

Sarthou, G., K. Timmermans, S. Blain, and P. Treguer (2005), Growth physiology and fate of diatoms in the ocean: a review, *Journal of Sea Research*, *53*, 25–42.

Schlitzer, R. (2000), Applying the adjoint method for biogeochemical modeling: Export of particulate organic matter in the World Ocean, in *Inverse methods in biogeochemical cycles*, *AGU Monograph*, vol. 114, edited by P. Kasibhata, pp. 107–124.

Six, K. D., and E. Maier-Reimer (1996), Effects of plankton dynamics on seasonal carbon fluxes in an ocean general circulation model, *Global Biogeochem. Cycles*, *10*, 559–583.

Smith, S. V., and J. T. Hollibaugh (1993), Coastal Metabolism and the oceanic organic carbon balance, *Rev. of Geophys.*, *31*, 75–89.

Soetaert, K., J. J. Middelburg, P. M. J. Herman, and K. Buis (2000), On the coupling of benthic and pelagic biogeochemical models, *Earth-Science Reviews*, *51*, 173–201.

Sommer, U. (1986), Nitrate and silicate competition among antarctic phytoplankton, *Mar. Biol.*, *91*, 345–351.

Stemmann, L., G. A. Jackson, and G. Gorsky (2004), A vertical model of particle size distributions and fluxes in the mid-water column that includes biological and physical processes-Part II Application to a three year survey in the NW Mediterranean Sea, *Deep Sea Res. Part I*, *51*, 885–908.

Strom, S. L., C. B. Miller, and B. W. Frost (2000), What sets lower limits to phytoplankton stocks in High Nutrient, Low Chlorophyll regions of the open ocean?, *Marine Ecology Progress Series*, *193*, 19–31.

Sunda, W. G., and S. A. Huntsman (1997), Interrelated influence of iron, light and cell size on marine phytoplankton growth, *Nature*, *390*, 389–392.

Takahashi, T., W. S. Broecker, and S. Langer (1985), Redfield ratio based on chemical data from isopycnal surfaces, *J. Geophys. Res.*, *90*, 6907–6924.

Takahashi, T., R. A. Feely, R. Weiss, R. H. Wanninkhof, D. W. Chipman, S. C. Sutherland, and T. T. Takahashi (1997), Global air-sea flux of CO_2: an estimate based on measurements of sea-air pCO_2 difference, in *Proceedings of the National Academy of Science*, vol. 94, p. 8929, National Academy of Science, USA.

Takeda, S. (1998), Influence of iron availability on nutrient consumption ratio of diatoms in oceanic waters, *Nature*, *393*, 774–777.

Tegen, I., and I. Fung (1995), Contribution to the atmospheric mineral aerosol load from land surface modification, *J. Geophys. Res.*, *100*, 18,707–18,726.

Tréguer, P., D. M. Nelson, A. J. Van Bennekom, D. J. DeMaster, A. Leynaert, and B. Quéguiner (1995), The silica balance in the World Ocean: A reestimate, *Science*, *268*, 375–379.

Wanninkhof, R. (1992), Relationship between wind speed and gas exchange over the ocean, *J. Geophys. Res.*, *97*, 7373–7382.

Yoshioka, Y., and Y. Saijo (1984), Photoinhibition and recovery of NH_4^+-oxidizing bacteria and NO_2-oxidinzing bacteria, *Journal of General and Applied Microbiology*, *30*, 151–166.